Mineral equilibria at high PT-parameters

Bulatov V.K.[1,3], Girnis A.V.[2,3], Brey G.P.[3], Woodland A.[3], Höfer H.[3] Ferropericlase cristallization under upper mantle conditions.

[1]V.I. Vernadsky Institute RAS, Moscow (v.bulatov@bk.ru.), [2]Institute of Geology of Ore Deposits, Petrography, Mineralogy, and Geochemistry RAS, Moscow (girnis@igem.ru.), [3]J.-W. Goethe Universität, Frankfurt am Main, Germany, woodland@em.uni-frankfurt.de, [3]Goethe Universität, Frankfurt am Main, Germany, (brey@em.uni-frankfurt.de.), [3]Goethe Universität, Frankfurt am Main, Germany. (hoefer@em.uni-frankfurt.de.).

Abstract. Ferropericlase is a common lower mantle phase that can occur as inclusions in "superdeep" diamonds. However, it has been proposed that some of these inclusions could be formed in the upper mantle (Brey et al. 2004). To explore this hypothesis, two types of experiments on ferropericlase crystallization were conducted at 5–12 GPa and 1500–1700 °C: (1) equilibrium experiments with Ca–Mg–Fe carbonate + MgO + olivine mixtures and (2) "sandwich" experiments containing a layer of metallic iron overlain by olivine, with a carbonate layer on top. The equilibrium experiments produced a series of carbonate–silicate melts saturated in olivine and ferropericlase. These melts contain 2–12 wt% SiO2, which correlates negatively with CaO and CO2 contents and positively with temperature. A comparison of the composition of the carbonate–silicate melts with literature data for melts saturated in olivine and low-Ca pyroxene indicate that melts saturated in ferropericlase cannot be produced by crystallization of melts derived by melting carbonated harzburgite or lherzolite at upper mantle conditions. On the other hand, the sandwich experiments reveal that ferropericlase and diamond (or metastable graphite) can crystallize simultaneously during the reduction of carbonate–silicate melt. The resulting ferropericlase crystallizing in equilibrium with olivine will be richer in Fe compared with lower mantle ferropericlase in equilibrium with bridgmanite. Thus, the considerable variation in Mg# values observed for some suites of ferropericlase inclusions in diamond could in part be attributable to ferropericlase formation in the upper mantle.

Keywords High-pressure experiment · Ferropericlase · Upper mantle · Carbonate–silicate melt · Crystallization · Diamond

Ferropericlase, (Mg,Fe)O, is one of the major phases in the lower mantle, which is indicated by experimental and seismological evidence (e.g., Helffrich and Wood, 2001). Its stability in the mantle is controlled by the reaction

$(Mg,Fe)_2SiO_4$(ringwoodite) = $(Mg,Fe)SiO_3$(perovskite) + (Mg,Fe)O(ferropericlase), (1)

which occurs at a pressure of ~23 GPa or a depth of ~660 km corresponding to one of the major seismic discontinuities in the mantle (Liu, 1975; Ito and Takahashi, 1989). At lower pressure, ferropericlase is unstable in peridotitic assemblages, because of its interaction with low-Ca pyroxene and formation of olivine (reaction 1 is shifted to the left). Therefore, ferropericlase inclusions in diamonds are believed to come from the lower mantle or transitional zone (Kaminsky, 2012, and reference therein). Ferropericlase (and much rarer magnesiowüstite) is the most common superdeep (lower mantle) mineral among inclusions in terrestrial diamonds.

In this paper we report experimental evidence on the possible mechanism of formation of ferropericlase inclusions in diamond under upper mantle conditions. Two types of experiments were performed at 5–12 GPa. (1) Equilibrium experiments aimed at determining the composition of carbonate-silicate melt coexisting with olivine and ferropericlase. (2) Experiments on reduction of carbonate-silicate melt under the influence of an external reducer. We sought to answer two questions: (1) can ferropericlase appear as a product of crystallization of carbonate-silicate melt derived from carbonated upper mantle peridotite at high pressure (within the diamond stability field); and (2) can ferropericlase co-crystallize with diamond during reduction of carbonate-silicate melt?:

In order to determine the composition of silicate-carbonate melt saturated in olivine and ferropericlase, equilibrium experiments with mixtures of Ca–Fe–Mg carbonates and excess olivine and periclase were conducted at 5–12 GPa and 1500–1700°C. Starting materials were prepared from natural magnesite, calcite, siderite and San Carlos olivine (mg# ~ 0.91) and chemical reagents Fe and MgO. Starting materials were loaded into Pt capsules (1.6 mm O.D. and 1.5–2.0 mm long) lined with Re foil to minimize Fe loss.

The experiments were performed in a Walker-type multianvil apparatus using tungsten carbide cubes with a truncation edge length of 8 mm. More details on the experimental apparatus and pressure calibration were reported by Brey et al. (2008). The duration of the experiments was from 1 to 52 h. The products were analyzed with a Jeol Superprobe 8900 electron microprobe. Minerals were analyzed with a focused beam, and quenched melts, with a beam defocused to a 20 μm spot size.

Figure 1 provides an example of run products in the equilibrium experiments. In all cases olivine and ferropericlase coexisted with carbonate-silicate melt. At 1500°C, the fraction of melt was relatively low, and partial melt distributed between mineral grains. At higher temperatures, a pool of quenched melt was observed in the upper part of the sample. Olivine in such experiments occurred in a polycrystalline aggregate below the melt zone. In contrast, a significant number of rounded ferropericlase grains usually remained suspended in the melt (Fig. 1). The

polycrystalline aggregate below the melt zone also contained rounded to irregular ferropericlase grains (Fig. 1). The melts are dominated by carbonate components. Their SiO_2 content is from 2 to 12 wt% and correlates positively

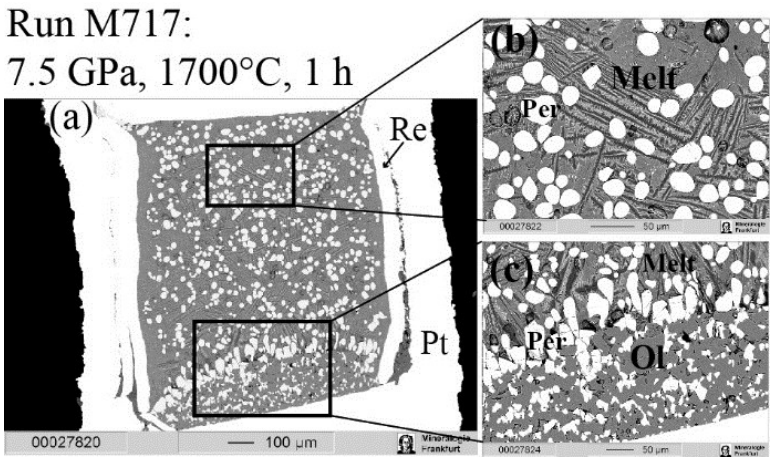

Fig 1. Back-scattered electron (BSE) images of products of a typical equilibrium experiment. A general view of the sample is shown in the left, and two enlarged parts are shown in the right. The sample consists of two zones: upper zone consisting of quenched melt and suspended ferropericlase grains (white) and lower zone of melt-free olivine-ferropericlase aggregate.

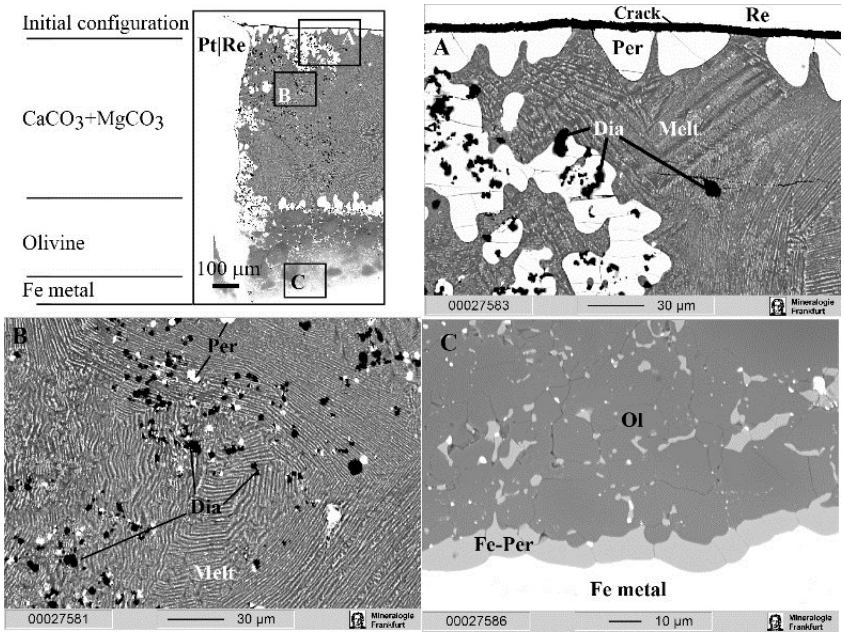

Fig. 2. BSE images of a sandwich experiment (M701 at 10.5 GPa, 1600°C, 1 h) showing an overview (upper right) and three enlarged fragments (A, B, and C). (A) Relatively large ferropericlase and diamond grains at the top of the capsule. (B) Simultaneous homogeneous nucleation of diamond and ferropericlase in carbonate-silicate melt. (C) The bottom of the olivine layer with a continuous wüstite film between olivine and metallic iron. Note also wüstite development along grain boundaries in the olivine layer.

with temperature and MgO+FeO and negatively with CaO and CO_2 Magnesite was observed in several runs at the bottom of the sample. In most cases, the minerals were homogeneous. Only in some experiments large olivine grains exhibited Fe-rich cores with mg# close to that of starting olivine and Mg-rich rims with mg# ~ 0.97. The difference between the compositions of ferropericlase grains suspended in melt and enclosed in the mineral aggregate below the melt was always negligible.

Sandwich experiments showed more heterogeneous structures and mineralogy (Fig. 2). The lowermost layer consisted of pure iron with small wüstite inclusions. Wüstite also occurred as a continuous layer between the iron and olivine zones and thin intergranular films in the lower part of the olivine zone (Fig. 2C). The phase assemblage of the

melt zone was variable. In run M689 (7.5 GPa, 1500°C, 2 h), small scattered graphite grains were observed near the top of the melt zone. In run M699 (7.5 GPa, 1500°C, 4 h), ferropericlase with mg# > 0.7 was formed in the melt zone above the olivine layer. The most interesting results were obtained in run M701 (10 GPa, 1600°C, 1 h), in which simultaneous formation of diamond and ferropericlase with mg# ~ 0.65 was observed in the upper part of the melt zone. Small (<5 □m) isometric diamonds and ferropericlase grains are dispersed in the melt zone away from other minerals and capsule walls (Fig. 2B).Larger (up to 30 □m) ferropericlase grains with numerous diamond inclusions were observed at the top of the melt zone near the upper Re lid (Fig. 2A). In longer experiments the amount of melt decreased and the Ca–Mg-silicate merwinite appeared in runs M695 and M743. These experiments contain also a few relatively large (up to 20 □m) diamond crystals. These observations indicate that diamond was formed together with ferropericlase through homogeneous nucleation in carbonate-silicate melt. At increasing experimental duration, the initial diamond grains recrystallized to larger crystals.

The SiO_2 and (Mg,Fe)O activities in melt in equilibrium with olivine and ferropericlase are buffered by the reactions

Mg_2SiO_4(olivine) = MgO(ferropericlase)+SiO_2(melt) and (2)

MgO(melt) = MgO(ferropericlase). (3)

The mole fractions of SiO_2 and MgO+FeO in carbonate-silicate melt are therefore functions of *P, T* and composition parameters accounting for the nonideality of silicate-carbonate melt. The examination of experimental data shows that there is a significant temperature effect on X_{SiO2} and $X_{(Mg,Fe)O}$ and the pressure influence is much less significant. In addition, there are strong negative correlations between X_{SiO2} and X_{CaO} and X_{CO2} and a positive correlation between X_{SiO2} and $X_{(Fe,Mg)O}$.

Unfortunately, there are very few data on the olivine–ferropericlase–carbonate-silicate melt equilibrium, and it is difficult to separate the influence of different parameters on melt composition. A comparison with melts in equilibrium with olivine and low-Ca pyroxene may be useful. In these melts, SiO_2 and MgO+FeO mole fractions are also buffered by the reactions

Mg_2SiO_4(olivine) + SiO_2(melt) = $MgSiO_3$(low-Ca pyroxene) and (4)

$MgSiO_3$(low-Ca pyroxene)+MgO(melt) = Mg_2SiO_4(olivine). (5)

The compositions of melts are very similar to those in equilibrium with olivine and ferropericlase and the effects of pressure, temperature and compositional parameters on SiO_2 and MgO+FeO mole fractions should be similar. Therefore, we analyzed the available data on carbonate-silicate melts in equilibrium with olivine and low-Ca pyroxene from experiments at 2–14 GPa. The data array included experiments with CO_2 contents constrained by mass balance or other considerations. The compositions of these melts exhibit tendencies similar to those observed in our experiments for melts in equilibrium with olivine and ferropericlase. There are also similarly strong effects of *T*, X_{CaO} and X_{CO2} on X_{SiO2} and $X_{(Mg,Fe)O}$. The fields of the two arrays can be separated in the multidimensional compositional space. In order to check this suggestion and take into account variations in all parameters, the SiO_2 and MgO+FeO mole fractions of melts in equilibrium with olivine and low-Ca pyroxene were approximated by the equation:

$$RT\ln(Y) = A + BT + CP + f(X_i), \quad (6)$$

where *Y* is either X_{SiO2} or $X_{(Mg,Fe)O}$, *T* is absolute temperature, *P* is pressure in bar, and $f(X_i)$ is a function of compositional parameters. Using the experiments from the above-cited publications, the following equations were obtained by the least squares fitting for the compositions of anhydrous carbonate-silicate melts saturated in olivine and orthopyroxene at 2–14 GPa:

$$RT\ln(X_{SiO2}) = 5830.5–40.671(T–273)– 73283X_{CaO}+289183X_{CO2}–527146X_{CO2}^2 \quad (7)$$

$$RT\ln(X_{(Fe,Mg)O}) = 19859.9+0.01998P–14.346(T–273)– 35467.5X_{CaO}–26569.9X_{CO2}. \quad (8)$$

where temperature (*T*) is in K, and pressure (*P*) is in bars. Similar to our results for melts saturated in olivine and ferropericlase, the temperature effect is much greater than that of pressure. Among the compositional parameters, CaO and CO_2 contents are most significant, and the effect of CO_2 on SiO_2 is strongly nonlinear. The influence of other components (i.e., alkalis, Al, etc.) are negligible or uncertain.

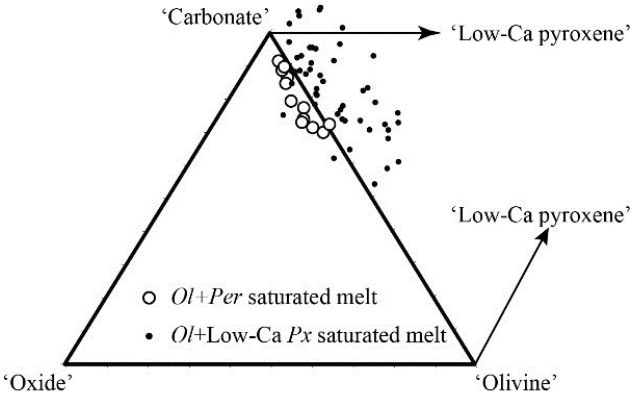

Fig. 3. Contents of normative components in experimental carbonate-silicate melts in equilibrium with either olivine and ferropericlase or olivine and low-Ca pyroxene at 5–12 GPa and 1200–1700°C. Ferropericlase-saturated melts are from this study, and low-Ca pyroxene saturated melts are from the literature.

Carbonate-silicate melts saturated in olivine and ferropericlase are systematically enriched in (Mg,Fe)O and depleted in SiO_2 compared with melts derived from carbonated harzburgite or lherzolite. The difference decreases with increasing pressure, and the compositions of melts in equilibrium with the two assemblages converge at ~12 GPa. However, there are very few data at pressures above 10 GPa, and any definite conclusion would be premature. The obtained relations suggest that carbonate-silicate melts saturated in olivine and ferropericlase can hardly be produced by olivine crystallization or dissolution from melts derived from carbonated peridotite, because this would change SiO_2 and MgO+FeO contents in the same direction.V To further support this conclusion, the melt compositions were recalculated to normative components: 'carbonate' = $2CO_2+NaO_{0.5}+KO_{0.5}$, 'olivine' = $3SiO_2$ and 'oxide' = CaO+FeO+MgO–0.5'carbonate'–0.67'olivine'.

Figure 3 shows that melts in equilibrium with olivine and low-Ca pyroxene have negative contents of the 'oxide' component (i.e., they are orthopyroxene-normative), whereas those in equilibrium with olivine and ferropericlase have 'oxide' > 0 (periclase-normative). The transition from orthopyroxene- to periclase-normative melts would require 'oxide' addition, which is not possible if olivine and carbonate are the only crystallizing phases. The only process resulting in the addition of normative 'oxide' is the dissolution of olivine with simultaneous crystallization of low-Ca pyroxene. However, this mechanism is infeasible up to pressures at which ferropericlase can coexist with a $(Mg,Fe)SiO_3$ phase.

Thus we conclude that the crystallization of melts derived from carbonated harzburgite or lherzolite cannot produce ferropericlase-saturated liquids under upper-mantle conditions. During decompression and cooling such melts will produce olivine, orthopyroxene and, eventually, magnesite.

An alternative scenario for an increase in $X_{(Fe,Mg)O}$ in carbonate-silicate melt involves partial CO_2 removal from the melt, which will result in transformation of 'carbonate' to 'oxide' components. Direct CO_2 degassing is hardly possible, because it would require very high temperatures of ~1700°C at 6–7 GPa (Girnis et al., 2011). A more realistic mechanism is partial reduction of carbonate-silicate melt with the formation of graphite or diamond through the schematic reaction

$MgCO_3$(melt) = MgO(periclase) + C(graphite/diamond) + O_2. (9)

Our sandwich experiments supported this mechanism and showed that reaction (9) can produce elemental carbon (diamond at 10 GPa and metastable graphite at 7.5 GPa) and ferropericlase. It is important that we avoided a direct contact between the melt and metal, in contrast to the experiments of Martirosyan et al. (2016) on $CaCO_3$–Fe interaction. In our experiments, metallic iron served as an external reducer and a sink for oxygen produced by redox reaction (9). The process in the melt layer is hence independent of the composition of the reducer, and the experiment can simulate natural diamond and ferropericlase formation in the absence of metallic iron. In nature, carbonate reduction can be caused, for instance, by the influx of a reduced fluid into the melt chamber or other mineral reactions. One necessary condition is the absence of orthopyroxene in the mineral assemblage, i.e., a dunitic environment. Ferropericlase that is formed locally in the upper mantle must differ from lower-mantle ferropericlase in mg# value. Experimental data on Fe–Mg partitioning between ferropericlase and wadsleyite or ringwoodite (Frost et al., 2001; Frost, 2003) show that mg# of ferropericlase in the pyrolytic mantle is not lower than 0.8. The partition of Fe and Mg between olivine and ferropericlase in our experiments is rather complex and depends on mg#. In all cases, K_D(Per-Ol) is much higher than 1, and experimental ferropericlase is strongly enriched in Fe relative to olivine and even melt. Ferropericlase in equilibrium with olivine with mg# of ~0.90 has mg# ~ 0.7. Hence, the contrast between the mg# of ferropericlase and $(Mg,Fe)_2SiO_4$ phases is much greater in the case of olivine than for wadsleyite or ringwoodite, and at the same bulk mantle composition, ferropericlase from the upper mantle will be richer in Fe than that from the lower mantle. Furthermore, the K_D(Per-Ol) is more sensitive to variations in mg# than K_D(Per-wadsleyite) and K_D(Per-ringwoodite), which suggests a stronger scatter of mg# values in upper mantle ferropericlase.

Ferropericlase inclusions in Juina diamond show the maximum range of mg# values (Kaminsky, 2012). The formation of Fe-rich ferropericlase and magnesiowüstite was attributed, in particular, to diamond crystallization at the lowermost mantle near the core–mantle boundary (e.g., Wirth et al., 2014; Kaminsky et al., 2015). However, at least some of the Juina diamonds were most likely formed at pressures of around 10 GPa, below the stability field of $CaSiO_3$ perovskite (Anzolini et al., 2016). Ferropericlase formation in the upper mantle in equilibrium with olivine provides an alternative provenance for low-mg# ferropericlase.

References

Abersteiner A, Kamenetsky VS, Pearson DG, Kamenetsky M, Goemann K, Ehrig K, Rodemann T (2018) Monticellite in group-I kimberlites: implications for evolution of parental melts and postemplacement CO2 degassing. Chem Geol 478:76. Anzolini C, Angel RJ, Merlini M, Derzsi M, Tokár K, Milani S, Krebs MY, Brenker FE, Nestola F, Harris JW (2016)

Depth of formation of CaSiO3-walstromite included in super-deep diamonds. Lithos 265:138–147.
Brey GP, Bulatov V, Girnis A, Harris JW, Stachel T (2004) Ferropericlase—a lower mantle phase in the upper mantle. Lithos 77:655–663.
Girnis AV, Brey GP, Bulatov VK, Höfer HE, Woodland AB (2018) Graphite to diamond transformation during sediment–peridotite interaction at 7.5 and 10.5 GPa. Lithos 310–311:302–313.
Helffrich GR, Wood BJ (2001) The earth's mantle. Nature 412:501–507.
Kaminsky F (2012) Mineralogy of the lower mantle: a review of 'superdeep' mineral inclusions in diamond. Earth-Sci Rev 110:127–147.
Kaminsky FV, Ryabchikov ID, McCammon CA, Longo M, Abakumov AM, Turner S, Heidari H (2015) Oxidation potential in the Earth's lower mantle as recorded by ferropericlase inclusions in diamond. Earth Planet Sci Lett 417:49–56.
Ito E, Takahashi E (1989) Postspinel transformations in the system Mg2SiO4–Fe2SiO4 and some geophysical implications. J Geophys Res 94:10637–10646.
Liu L (1975) Post-oxide phases of olivine and pyroxene and mineralogy of the mantle. Nature 258:510–512.
Martirosyan NS, Litasov KD, Shatskiy A, Ohtani E (2015) The reactions between iron and magnesite at 6 GPa and 1273–1873 K: implication to reduction of subducted carbonate in the deep mantle. J Mineral Petrol Sci 110:49–59
Palyanov YN, Bataleva YV, Sokol AG, Borzdov YM, Kupriyanov IN, Reutsky VN, Sobolev NV (2013) Mantle–slab interaction and redox mechanism of diamond formation. Proc Nat Acad Sci 110:20408–20413
Seitz H-M, Brey GP, Harris JW, Durali-Müller S, Ludwig T, Höfer HE (2018) Ferropericlase inclusions in ultradeep diamonds from Sao Luiz (Brazil): high Li abundances and diverse Li-isotope and trace element compositions suggest an origin from a subduction mélange. Mineral Petrol https ://doi.org/10.1007/s0071 0-018-0572-0.
Stachel T, Harris JW, Brey GP (1998) Rare and unusual mineral inclusions in diamonds from Mwadui, Tanzania. Contrib Mineral Petrol 132:34–47.
Stachel T, Harris JW, Brey GP, Joswig W (2000) Kankan diamonds (Guinea): II. Lower mantle inclusion paragenesis. Contrib Mineral Petrol 140:34–47.
Xu XZ, Yang JS, Robinson PT, Xiong FH, Ba DZ, Guo GL (2015) Origin of ultrahigh pressure and highly reduced minerals in podiform chromitites and associated mantle peridotites of the Luobusa ophiolite, Tibet. Gondwana Res 27:686–700.

Fedkin V.V., Sipavina L.V. Clinopyroxen in the eclogite-blueschist complexes: structural signs of the conditions of its formation UDC 549.6+552.16:552.48

D.S. Korzhinskii Institute of Experimental Mineralogy RAS (IEM) Chernogolovka, vfedkin@iem.ac.ru

Abstract. Nuclear gamma resonance (NGR) and X-ray powder diffractometry (XRD) methods have been used to study the fine structural organization of omphacite, one of the main indicators of metamorphism conditions. A detailed study of clinopyroxenes from eclogites of the Atbashy (South Tien Shan) and Maksyutov (South Urals) complexes, contrasting in depth, allows comparing the features of local fields in the mineral structure and relating them to the physicochemical conditions of the complexes formation. In the At-47 omphacite from the eclogite of the Atbashy complex, along with the M1 doublet, known for hedenbergite, the configurations typical for diopside (M1a doublet) are more noticeable, and the Maksyutov eclogite sample Mks-110 is characterized by the M1b jadeite doublet. The presence in the spectrum of the last omphacite of a significant fraction of M1 polyhedra (M1b doublet) with parameters characteristic of the high-pressure non-preserved structure of clinoferrosilite and jadeite can be a sign of the high-pressure origin of the studied omphacites. The data obtained confirm the presence of a mutual ordering effect at the M1 and M2 positions of cations with a contrasting size and different charge, which is expected for omphacite. Direct evidence of the preference for local configurations of M3 + (M1) - M1 + (M2) clarifies the physical motives of the cation ordering during pyroxene transformations associated with a change in their local electronic structure. An analysis of the results for the first time reveals the important role of the boundaries of the topological stability of pyroxene structures in their transformations at high pressures and makes it promising to use the identified features to assess the depth of formation of the eclogite-blueschist complexes.

Keywords: *UHP metamorphic complex, Maksyutov complex, Atbashy complex, depth of formation, nuclear gamma resonance (NGR), X-ray powder diffractometry (XRD) methods, fine structural organization of omphacite*

Assessment of the parameters of mineral formation and the evolution of the metamorphism of eclogite-blueschist complexes is carried out, as a rule, using mineral equilibria with the participation of omphacite. A detailed study of this mineral by the methods of nuclear gamma resonance (NGR) and X-ray powder diffractometry (XRD) showed the presence of a fine structural organization in it (Novikov, Sipavina, Sokolov, 1999; Novikov, Sipavina, Fedkin, 2007; Fedkin et al., 2007). These features were studied in clinopyroxenes from eclogites, contrasting in the physicochemical conditions of the formation of the Atbashy (South Tien Shan) and Maksyutov (South Urals) complexes. The revealed correlations between the pyroxene structures and PT parameters of the formation of high-pressure rocks are another criterion for assessing the depth of their origin.

According to Miyashiro's concept of paired metamorphic belts, the Maksyutov and the Atbashy eclogite-blueschist complexes are included in the system of the inland Ural-Tien Shan Hercynian fold belt and are connected with its various branches - external and internal, respectively. **The Maksyutov complex** is located in the zone of the Main Ural Fault and traces the zone of junction of the East European platform and the Magnitogorsk island arc. Its main

feature is the presence of ultrahigh pressure (UHP) mineral assemblages in the eclogite-blueschist rocks: microinclusions of diamond in rock-forming minerals, quartz pseudomorphs after coesite, and graphite cuboids after diamond. This determines the maximum metamorphism parameters in the region of diamond and coesite stability and at the early stage of complex development could reach T = 650-700oC and P = 2.7-3.2 GPa (Valizer et al., 2015; Fedkin et. al 2017; Fedkin 2020). Subsequent retrograde and repeated progressive stages of metamorphism occurred under the conditions of blue schists (T ~ 450-700 ° C, P ~ 1.2-1.7 GPa) and greenschist facies (T ~ 380-470 ° C, P ~ 0.7-1.3 GPa). The age of the main stage of eclogite metamorphism is estimated as Late Paleozoic - 375-390 Ma. However, some researchers note an earlier, Early Paleozoic stage of complex formation - 533 ± 4.6 Ma, and see this as its two-stage development (Shatsky et al., 1997, Valizer et al., 2015).

The Atbashy eclogite-blueschist complex is confined to the most important tectonic border between the northern and southern Tien Shan - the deep fault of Kansk -Atbashy and forms the Precambrian basement of the Hercynian folded system. Detailed petrographic studies of eclogite-blueschist and other accompanying rocks included in the Cheloktor suite show that these rocks formed under moderate (up to 1.2-1.3 GPa) pressure and intermediate temperatures of 400-700 ° C (Dobretsov, Sobolev, 1977). Progressive zonation of garnet and retrograde transformation of rocks (glaucophane growth, muscovitization, carbonization, etc.) are interpreted from the point of view of intense acid leaching, metasomatism against the background of ongoing metamorphic processes. The available petrochemical data and the observed sequence of mineral reactions occurring during the retrograde transformations of highly metamorphosed rocks (eclogites and garnet-clinopyroxene rocks) into glaucophane-containing and muscovite-quartzite schists, indicate that the chemical composition of the rocks of the complex at different stages of metamorphism changed at decrease in the content of Ca, Mg, and Fe oxides, at gradual increase in the contents of Si, Al, and K oxides and an increase in sodium activity. The age of metamorphism of eclogite-blueschist rocks of the complex is defined as 320-360 Ma (Dobretsov, 1974), although there are more ancient dating - 520-550 and even 1100 Ma. The consecutive transition from eclogites to Grt-Gln rocks, quartzite schists, and chlorite diaphthorites builds up a trend typical for regions of intercontinental suture structures to change the PT conditions of the clockwise metamorphism with a low (~ 10 deg / km) geothermal gradient at the initial stage of development and maximum parameters up to T = 650-700^{o}C at P = 1.4-1.5 GPa (Fedkin, 2004). The minimum PT conditions of mineral formation in the rocks of the Atbashy complex are fixed at the level of the green shale facies in the form of regressive PT trends from T = 550-570 ° C and P = 0.3-0.5 GPa to T = 350-400 °C at P = 0.05-0.2 GPa. The progressive orientation of metamorphic processes recorded in the zonality of garnet. The retrograde transformation of rocks took place against the background of intensive acid leaching and magnesia metasomatism.

The study of clinopyroxene from eclogite-blueschist complexes contrasting depth of formation allowed us to compare the features of the structure of the mineral with the physicochemical conditions of the origin of the host rocks. The studies were carried out by the methods of X-ray powder diffractometry (XRD) and nuclear gamma-resonance (NGR) in model systems of solid solutions of Ge-Si pyroxene. The Si → Ge substitution in tetrahedral "removes from the shadows" high-pressure structures of clinopyroxenes, which are not retained during quenching, significantly expands the range of changes in the unit cell volume and makes it possible to study their features under normal conditions. For a comparative analysis of the structural modifications of monoclinic pyroxenes, the method of topological niches was used. For each of the structures, the scattering regions of the unit cell parameters were determined in the parameters - volume coordinates (a, b, c, β - V). Structural transformations were provoked by the selective replacement of cations in three positions - M1, M2, and tetrahedra, which allows not only determining the niches of topological stability of individual structures, but also obtaining important information about the nature of these transformations **(Novikov et al., 2004, 2005).**

Figure 1a shows topological niches for pyroxenes with a large cation size at position M2, Aeg structure C2 / c-III; for pyroxene systems with divalent cations, Hd structure C2 / c-II; and structures of omphacite P2 / n with multivalent ions and with an average polyhedron size M2. It was previously shown that in the hedenbergite structure, the Ca → Na and Ca → Fe substitutions at the M2 position have a gap, i.e. the final members of these series belong to various structural modifications — C2 / c-II and C2 / c-III (**Novikov et al., 2004).** These two structures are separated by the Jad-Om-Di trend niche (space group P2 / n), within which three intervals stand out, the narrowest of which on the unit cell volume scale belongs to omphacite.

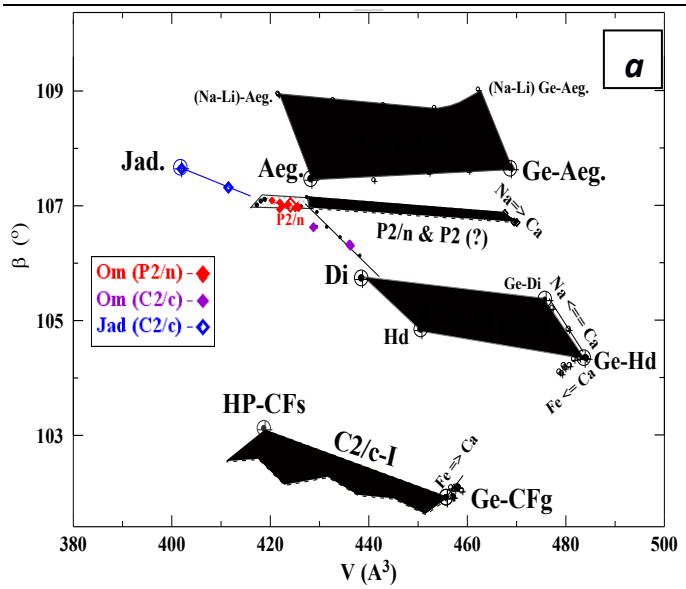

Fig. 1a. Topological β-V (A3) niches of five structures C2/cI, C2/c-II, C2/c-III, C2/c-IV, and P Ge-Si pyroxene solid solutions and three sections of the general trend β-V for natural pyroxenes solidsolution Jad-Aeg-Di, corresponding to three structural modifications: Jad, P-Omphacite (Om. P2/n – great rhomb) and Di.

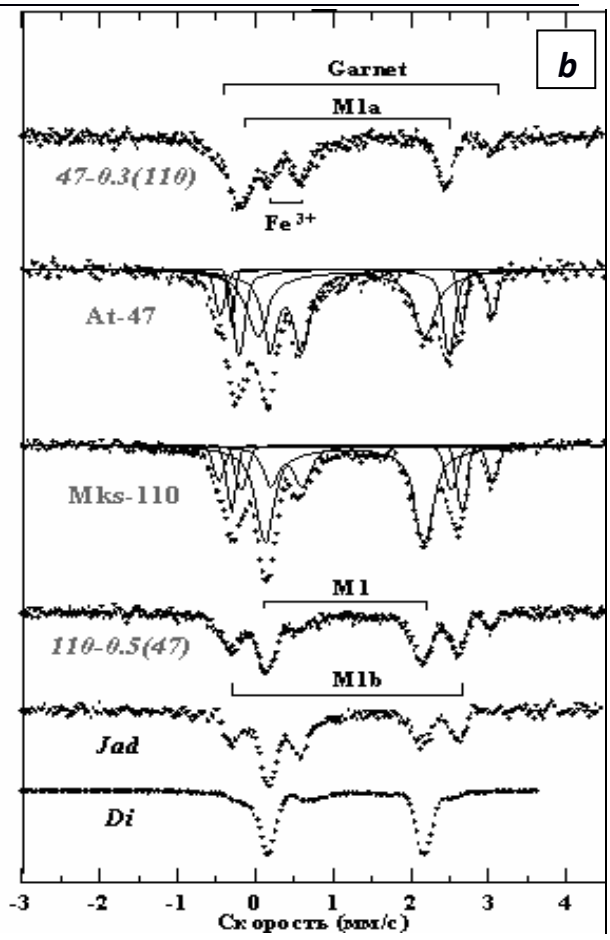

Fig. 1b. NGR spectra of omphacites from the eclogites of the Atbashy (At-47, X_{Jad}=0.16-0.36) and the Maksyutov (Mks-110, X_{Jad}=0.43-0.50) complexes, their difference spectra and the isolated spectra of jadeite and diopside.

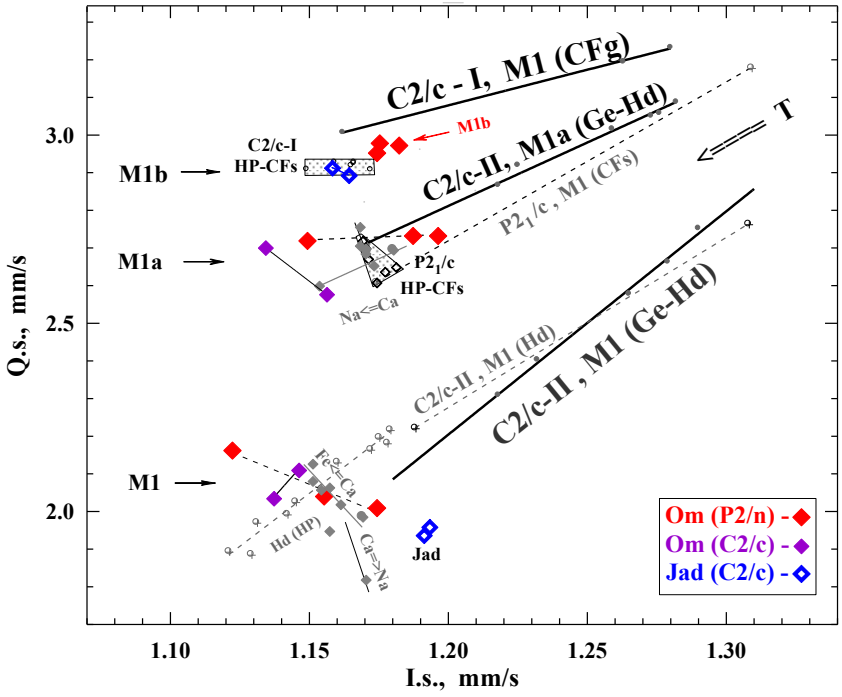

Fig.2. X-trends "Q.s. – I.s." for the main M1 and, M1a, M1b doublets: Omphacites and Clinopyroxenes. 300K: HP-CFs (C2/c-I and P21/c), HP-Hd, Jad, C2/c, Na- and Fe-substituted Ge-Hd (C2/c-II). 90-300K: Cpx P21/c, Hd (C2/c-II), Ge-Hd (C2/c-II), Fe- substituted Ge-Hd (C2/c-II; Ca0.8Fe 0.2).

Studies of local fields in the key structural position M1, carried out by the NGR method, significantly clarify the situation. The correct interpretation of the gamma-resonance spectra of omphacites **(Fig. 1b**) is difficult due to the presence of very close components. The application of the procedure for narrowing them significantly simplifies the problem, and in its spectra it is possible to determine two very close doublets with parameters coinciding with the parameters of the doublets M1a and M1b characteristic of diopside and jadeite - structures C2 / c-II and C2 / c-I, respectively **(Fig. 2).**

This allowed us to conclude (Novikov et al., 2005) that two different cationic M1 – M2 – T configurations are present in the P2 / n omphacite structure. One of them is characteristic of the jadeite structure (and then this is the Al3 + -Na1 + -Si configuration and it corresponds to the doublet of Fe2 + M1b ions), the second to the Di-Hd structure (Mg-Ca-Si configuration and the other doublet of Fe2 + ions are M1a). The foregoing makes it possible to consider the structure of omphacite bearing the characteristic features of three crystal-chemical end members (minals) with limited mutual miscibility and a hybrid structure (Novikov et al., 2007).

Comparative analyses of local fields in natural Omphacite, Jadeite and Di-Aeg solid solutions. In the key position M1, several discrete electronic states of Fe2 + ions are determined. X-trends QS-IS (quadrupole splitting - isomer shift) of Fe2 + ions with Ca, Fe, or Na ions in neighboring M2 positions fall into the niches of three different monoclinic structures of germanates with sp. Gr. C2 / s (**Novikov, 2004).** In addition to the main M1 (Hd) doublet, two more were determined in the NGR spectra of such pyroxenes: the M1a doublet (in structures P21 / c, P2 / n and C2 / c-II) and the M1b doublet (in structures C2 / cI, P2 / n, and Jad), moreover, only in omphacites with space group P2 / n there are precisely such three configurations: X (M2) = Ca, Fe, and Na. Their appearance in the M1 position of the pyroxene structures of Fe2 + ions with different electronic structures substantially supplements the idea of the local structure of mixed crystals.

The study of omphacites from the eclogites of the Atbashy and Maksyutov complexes made it possible to compare the features of local fields in them and relate them to structural features. In the At-47 omphacite from the eclogite of the Atbashy complex with a moderate content of the jadeite component (XJad = 0.16-0.36), along with the M1 doublet, known for hedenbergite, the configurations typical for diopside (M1a doublet) are more noticeable. The Maksyutov eclogite Mks-110 (XJad = 0.43-0.50) is characterized by the M1b jadeite doublet (Fig. 1b). The presence of a significant fraction of M1 polyhedra (M1b doublet) in the spectrum of the last omphacite with parameters characteristic of the high-pressure non-conserved structure of clinoferrosilite and jadeite can be a sign of high-pressure origin of the studied omphacites.

The data obtained confirm the presence of a mutual ordering effect at the M1 and M2 positions of cations with a contrasting size and different charge, which is expected for omphacite. An analysis of the results obtained for the first time reveals the important role of the boundaries of the topological stability of pyroxene structures in their transformations at high pressures and temperatures. Direct evidence of the preference for local configurations of M3 + (M1) - M1 + (M2) clarifies the physical motives of the cation ordering during pyroxene transformations associated with a change in their local electronic structure. The local ordering phenomenon M1-M2 induces the P2 / n => C2 / c transition, which depends on T and P and can be used both to analyze the structural features of cation ordering in natural omphacites and as a promising PT history sensor, formation eclogite-blueschist complexes.

The authors are extremely grateful to Dr. Ph. of Physical and Mathematical Sciences. G.V. Novikov, the initiator and head of structural studies of clinopyroxene, which form the basis of the petrological interpretation of the results. This work was supported by the Russian Foundation for Basic Research (grants 05-05-64561, 05-07-90318) and the Fulbright Program of the Institute of International Education (grants 2011 and 2015).

References

1. Dobretsov N. L., Shatsky V. S., Coleman R. G., Lennykh V. I., Valizer P. M., Liou J. G., Zhang R. and Beane R. J., (1996) Tectonic Setting of Ultrahigh-pressure Metamorphic Rocks in the Maksyutov Complex, Ural Mountains, Russia. International Geology Review, 1996, v. 38, p. 136-160.
2. Dobretsov, N.L., Sobolev N.V. Blueschist Belts. In: "Metamorphic complexes of Asia". Novosibirsk. "Nauka". 1977. p.283-288. (in Russian).
3. Dobretsov, N.L., 1974. Blueschist and Eclogite– Blueschist Complexes of the USSR. Ed. V.S.Sobolev Novosibirsk. "Nauka". Iss.57. 430p. (in Russian).
4. Fedkin et al., (2017) Coexisting Zoned Garnets and Clinopyroxenes from Mafic Eclogites of the Maksyutov Complex, South Ural Mountains, Russia. // Experiment in Geosciences. V. 23. No 1. P. 5-13.
5. Fedkin V.V. Mineralogical geothermobarometry in developing metamorphic systems. // In: "Experimental Mineralogy: Some Results at the Turn of the Century." M. Science. 2004, v. 2, p. 172-187. (in Russian).
6. Fedkin V.V. Four Stages of the Thermal Evolution of Eclogites from the Maksyutov Complex (South Urals). // Geology and Geophysics (2020) Vol. 61, No. 5-6, pp. 543–558.
7. Fedkin V.V., Novikov G.V., Sipavina L.V., Fedkin A.V. (2007) Geochemical features of eclogite-blueschist rocks of the Maksyutov (Southern Urals) and Atbashy (Southern Tien Shan) complexes. // V All-Russian meeting "MINERALOGY OF URAL-2007" (August 20-25, 2007 Miass). Reports. C. 17-22. (in Russian).
8. Novikov G.V., Fedkin V.V., Sipavina L.V. Peculiarities in the structure and local fields in omphacites from the Maksyutov and Atbashy blueschist-eclogite complexes. // Experiment in Geosciences @ISSN 0869-2904.
9. Novikov G.V., Koshchug D.G. and Rager H. Alternative analysis of room temperature IR spectra of

quartz. (1997) Proceedings of the 39th International Geological Congress, Netherlands. 217-221.
10. Novikov G.V., Sipavina L.V., and Fed'kin V.V. (2007) Pyroxenes: Structural Transformations, Local Fields, and Effects of Short-Range Ordering of Cations. ISSN 1062-8738, Bulletin of the Russian Academy of Sciences: Physics, 2007, Vol. 71, No. 9, pp. 1305–1309. © Allerton Press, Inc., 2007.
11. Novikov G.V., Sipavina L.V., Fedkin V.V. (2005) Local structure and phase transformations in pyroxene systems. // In: "Spectroscopy, radiography and crystal chemistry of minerals." Materials Intern. Conf. Kazan: Pluto, p. 187. (in Russian).
12. Novikov G.V., Sipavina L.V., Sokolov Yu.A. Comparative crystal chemistry of mantle silicate and their structural analogs. Experiment in Geosciences. (1999) № 8, C.88-90.
13. Shatsky, V.S., Jagoutz, E., Koz'menko, O.A., 1997. Sm–Nd dating of high-pressure metamorphism of the Maksyutov Complex, South Urals. Dokl. Akad. Nauk 352 (6), 285–288. (in Russian).
14. Valizer, P.M., Krasnobaev, A.A., Rusin, A.I., 2013. Jadeite–grossular eclogite of the Maksyutov Complex, South Urals. Litosfera 4, 50–61.
15. Valizer, P.M., Krasnobaev, A.A., Rusin, A.I., 2015. UHPM eclogite of the Maksyutov Complex (Southern Urals). Dokl. Earth Sci. 461 (3), 291–296.

Gorbachev N.S., Kostyuk A.V., Nekrasov A.N., Gorbachev P. N., Sultanov D.M. The interaction of phlogopite with carbonate at *P* =4 GPa, *T*=1200–1300 °C: phase relationships and stability of phlogopite. UDC 550.4.02

D.S. Korzhinskii Institute of Experimental Mineralogy RAS
142432 Akademica Osip'yana str., 4, Chernogolovka, Moscow district. gor@iem.ac.ru, nastya@iem.ac.ru, alex@iem.ac.ru, dill@iem.ac.ru, p_gor@mail.ru

Abstract. The phase relations in the phlogopite-carbonate system were studied at P = 4 GPa, T = 1200 and 1300 °C. The solidus of Phl-Cb association was less than 1200 °C. The quenched samples had a zonal structure. The central part was characterized by a massive texture formed by the polymineral association of Phl–Grt–Cpx–MgSp–Ap formed as a result of the phlogopite reaction with carbonate and silicate-carbonate melt: 1) $2KMg_3AlSi_3O_{10}(OH)_2^{Phl}$ + $3(CaCO_3)^L = 3CaMgSi_2O_6^{Cpx} + MgAl_2O_4^{Sp} + (2MgCO_3 + K_2CO_3)^L + 2H_2O^{Fl}$. 2) $4KMg_3AlSi_3O_{10}(OH)_2^{Phl}$ + $4{,}5(CaCO_3)^L = 4{,}5CaMgSi_2O_6^{Cpx} + MgAl_2O_4^{Sp} + Mg_3Al_2Si_3O_{12}^{Grt} + (3{,}5MgCO_3 + 2K(OH))^L + 3H_2O^{Fl} + K_2CO_3^L$. The outer part of the experimental sample consisted of quenching phases of silicate-carbonate melt, consisting of different degrees of oriented elongated crystals of Phl, fouling with Ca-carbonate.

Keywords: phlogopite, carbonate, experiment, phase relations

Introduction. Phlogopite (Phl) is the most common dark-colored potassium-containing silicate in the crust and upper mantle. It is a potassium concentrator, as well as chlorine, fluorine, and water. As an accessory mineral, phlogopite is found in igneous rocks of various genesis. In the rocks of platform carbonatite-containing intrusive complexes of ultrabasic, basic and alkaline rocks, such as Kovdor, the concentrations of phlogopite are so high that they are industrial deposits. Phlogopite is also an important indicator of mantle metasomatism, as evidenced by its wide development in xenoliths of metasomatized peridotites and eclogites (O'Reilly, Griffin, 2013; Konzett et al., 2000). The appearance of phlogopite in such xenoliths is due to its formation as a result of interaction with potassium aqueous fluids (Misra et al., 2004). A review of the reactions occurring in this interaction according to natural and experimental data was made in work (Safonov, Butvina, 2016). Experimental modeling of the formation of phlogopite in the interaction of peridotite with potassium fluids at high pressures is given in a number of papers (Brey et al., 2011; Sokol et al., 2017). It was established that at 3 GPa the main phase, the decomposition of which leads to the formation of phlogopite, is garnet. In model and natural systems with H_2O or $H_2O + CO_2$ fluid in the range T = 1250–1300 °C with $P > 4$ GPa, the stability of phlogopite and carbonate is limited to near-solidus reactions such as phlogopite + enstatite + magnesite = forsterite + pyrope + K-C-O-H (silicate-carbonate melt). In association with carbonates, alkaline and kimberlite melts, phlogopite is noted to be stable to pressures greater than 7 GPa. Phlogopite phase relationships with some metasomatized upper mantle minerals, such as enstatite, diopside, garnet, magnesite, diopside + enstatite) were considered in the work (Frost, 2006; Enggist, Luth, 2016; Girnis et al., 2006). The purpose of this work is experimentally study the phase relationships and the geochemistry of the interaction of phlogopite with carbonate melts under dry conditions and with $H_2O + CO_2$ fluid in the range of 1200–1300°C.

Experimental and analytical methods. The experiments were carried out in Pt ampoules on anvil-with-hole apparatus (NL – 40) in IEM RAS using the quenching technique. Powders of specially prepared mixtures consisting of phlogopite (Phl) and carbonate fraction (Cb) were placed into Pt ampoule, which is hermetically sealed. Mixture composition are 90 wt.% of calcite carbonatite from the intrusive complex of ultrabasic, basic and alkaline rocks of Kovdor; 5 wt.% of Na_2CO_3 and 5 wt.% of K_2CO_3. The ratio of Na_2O/K_2O = 0,74. The weight ratio of Phl – Cb is 1 : 1. The temperature was measured by $Pt_{70}Rh_{30}/Pt_{94}Rh_6$ thermocouple. The pressure at high temperatures was calibrated using quartz – coesite equilibrium. The accuracy of determining the temperature and pressure in experiments is estimated at ± 5 °C and ± 1 kbar (Litvin, 1991). The duration of the experiments was 6–8 hours. Polished preparations of experimental samples were studied and analyzed using a TESCAN VEGA II XMU

electron scanning microscope equipped with a secondary and reflected electron detector and an INCA Energy 450 energy dispersive spectrometer and an INCA WEVE wave dispersion spectrometer.

Results. By texture and phase composition of the samples quenched at 1200 and 1300 °C, the central and boundary zones are distinguished with a clear boundary between them. The Central zone (I), reactionary, composes a matrix of the sample, with a massive texture, consisted of splices of crystals of phlogopite, clinopyroxene, carbonate, with inclusions of single crystals of spinel, garnet and apatite (Fig. 1a, 2a). In the matrix are large (100 x 200 microns) tabular shape of the original relics of phlogopite with inclusions of clinopyroxene. Clinopyroxene of augite composition with high Al_2O_3 content (up to 12 wt.%) contains impurities Na_2O, up to 0.8 wt.%, Sr_2O to 0.4 wt.%, TiO_2 to 0.5 wt.%. Garnet of pyrope-almandin-grossular composition X_{Mg}= 0,31, X_{Ca} = 0,58, X_{Fe} = 0,11 forms intergrowths with clinopyroxene and carbonate. Spinel occurs as idiomorphic inclusions in the bulk of the sample, contains FeO 4–5 wt.%.

The boundary zone (II) of the sample, confined to the contacts with Pt ampoule, formed by the carbonate melt quenching products, consists of isolated, elongated plates, about 20 x 300 mkm, with parallel orientation, sometimes forming a lattice texture. Their phase composition depends on the temperature. At 1200 °C, the plates consist of calcite carbonate composition, the edge parts of which are overgrown with needle-shaped micro-crystals of phlogopite and isolated apatite crystals (Fig. 1b). At 1300 °C with similar texture, tempered sample in the boundary zone is dominated by phlogopite, in the interstices of which are localized carbonate with crystals of apatite (Fig. 2b).

Features of the texture and phase composition of the experimental samples indicate that during the experiment in the process of peritectic melting as a result of the interaction of phlogopite (Phl) with the melt (L) and fluid (Fl) formed a polymineral association of phlogopite–carbonate–clinopyroxene–spinel±garnet and carbonate melt composition. Its formation can be represented by reactions: 1)

$$2KMg_3AlSi_3O_{10}(OH)_2^{Phl} + 3(CaCO_3)^L = 3CaMgSi_2O_6^{Cpx} + MgAl_2O_4^{Sp} + (2MgCO_3 + K_2CO_3)^L + 2H_2O^{Fl}.$$ 2)

$$4KMg_3AlSi_3O_{10}(OH)_2^{Phl} + 4{,}5(CaCO_3)^L = 4{,}5CaMgSi_2O_6^{Cpx} + MgAl_2O_4^{Sp} + Mg_3Al_2Si_3O_{12}^{Grt} + (3{,}5MgCO_3 + 2K(OH))^L + 3H_2O^{Fl} + K_2CO_3^L.$$

During the experiment, the carbonate melt migrates from the crystal matrix and concentrates on the border with the walls of the Pt ampoule. When quenching the melt, elongated crystals are formed, which are represented at 1200 °C mainly by carbonate, at 1300 °C by phlogopite and carbonate. By scanning the sample area, the compositions of the melts were evaluated (Table 1). With an increase in temperature from 1200 to 1300 °C and the degree of melting, the melt is enriched with components of phlogopite – Si, Ti, Al, Mg, K, and is depleted in Ca, a carbonate component, while the K_2O / Na_2O ratio increases from 2 to 5,4.

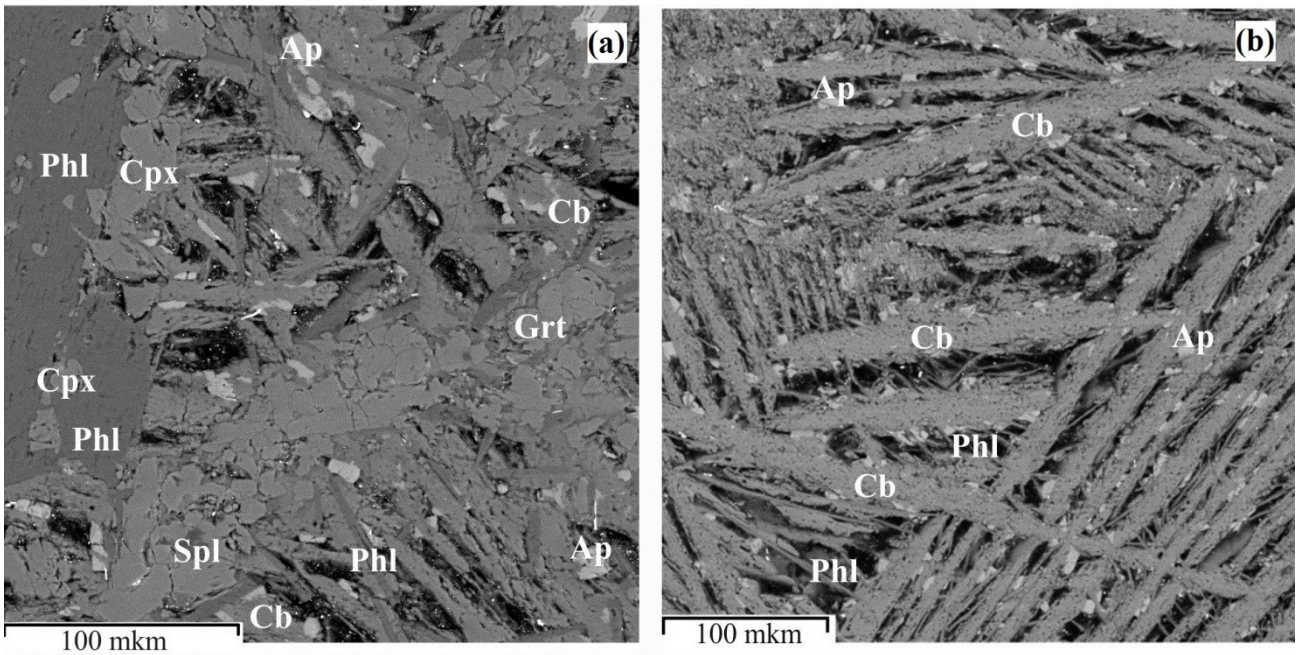

Fig. 1. BSE photo of the experimental sample in the phlogopite-carbonate system at 1200 °C. (a) Polymineral association of restite and newly formed phases of the central part of the sample, formed by the interaction of phlogopite with a carbonate melt; (b) quenched melt, xenomorphic, elongated carbonate crystals (Cb), overgrown with phlogopite needle crystals (Phl) and apatite microcrystals (Ap).

Table 1. Chemical compositions of coexisting phases in the phlogopite system at 1200–1300° C

	SiO_2	TiO_2	Al_2O_3	FeO	MgO	CaO	Na_2O	K_2O	Sr_2O	P_2O_5	Total
1200 °C, dry conditions											
Phl (I)	38.25	1.31	17.41	0.93	23.53	0.92	0.12	10.02	0.39	0.14	93.20
Phl (II)	25.14	1.40	9.00	1.79	21.91	7.66	0.57	9.06	0.59	2.26	79.35
Cb (I)	0.54	0.12	0.21	0.18	5.94	45.22	0.30	1.19	0.54	0.03	54.63
Cb (II)	3.85	0.22	1.75	0.39	6.69	40.71	0.27	1.75	0.43	0.51	56.69
Cpx (I)	47.28	0.49	12.37	1.60	12.95	23.31	0.68	0.14	0.34	0.10	99.40
Grt (I)	39.96	0.66	21.55	3.52	12.35	19.49	0.11	0.15	0.14	0.03	98.29
Spl (I)	0.87	0.02	66.85	4.66	24.87	0.38	0.20	0.03	0.21	0.00	98.58
Ap (I)	0.53	0.12	0.14	0.99	2.61	43.98	3.06	3.00	1.21	28.36	85.28
L	5.80	0.46	2.35	0.89	9.22	30.19	0.78	3.98	0.32	2.57	57.11
1300 °C, dry conditions											
Phl (I)	38.70	1.07	14.79	0.22	24.88	2.32	0.20	10.56	0.13	0.06	93.03
Phl (II)	38.52	0.87	16.11	0.63	24.36	1.50	0.09	10.60	0.30	0.1	93.15
Cb (I)	0.22	0.05	0.04	0.00	3.78	49.90	0.00	0.60	0.68	0.06	55.40
Cb (II)	0.42	0.04	0.12	0.21	2.78	48.80	0.47	1.17	0.61	1.35	56.11
Cpx (I)	47.42	0.44	13.17	2.64	12.84	24.19	0.75	0.03	0.17	0.07	101.85
Grt (I)	42.16	0.13	23.82	1.77	16.54	16.98	0.12	0.13	0.00	0.00	101.82
Spl (I)	0.72	0.00	68.64	3.96	26.35	0.23	0.00	0.00	0.42	0.00	100.69
Ap (I)	1.27	0.00	0.03	0.12	1.95	48.80	1.79	1.30	0.95	27.87	84.27
L	14.89	0.72	4.94	0.52	12.81	21.78	1.23	6.71	0.12	1.71	66.20

Note. Roman numerals at the phase index indicate its affiliation to the reactionary matrix (I) or to the quenched melt (II). Phl – phlogopite, Cpx – clinopyroxene, Spl – spinel, Ap – apatite, Cb – carbonate, L – melt.

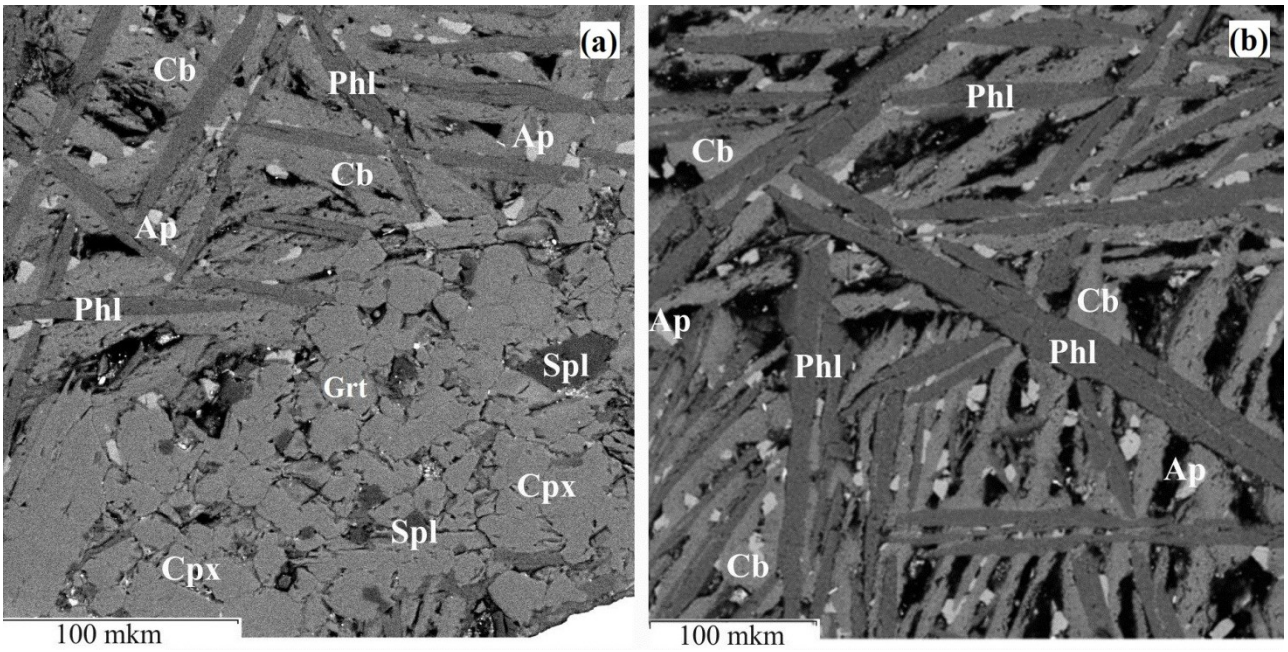

Fig. 2. BSE photo of the experimental sample in the phlogopite-carbonate system at 1300 °C. (a) Contact of the mineral association of restitic and newly formed phases, formed by the interaction of phlogopite and carbonate melt with quenched melt; (b) quenched melt, various forms of ratios of phlogopite (Phl) and carbonate (Cb).

Thus, in the phlogopite – carbonate system, in the process of peritectic melting, the interaction of phlogopite with carbonate melt results in the formation of mineral association of phlogopite + carbonate + diopside ± garnet + spinel and carbonate melt. At *P–T*, close to the mantle adiabat (4 GPa, 1300 °C), phlogopite remains stable in the presence of alkaline-carbonate fluids and silicate-carbonate melts.

The reported study was funded by RFBR, project number 17-05-00930a

References

Brey G.P., Bulatov V.K., Girnis A.V. Chem. Geol. 2011. V. 281. P. 333–342.

Enggist A., Luth R.W. Contrib Miner Petrol. 2016. 171(11):88.

Frost D.J. Reviews in Mineralogy and Geochemistry. 2006. V. 62(1). P. 243–271.
Girnis A., Bulatov V., Lahaye Y., Brey G. Petrology. 2006. V. 14. P. 492–514.
Konzett J., Armstrong R.A., Günther D. Contrib.Mineral.Petrol. 2000. V. 139. P. 704-719.
Litvin Yu.A. Physical and chemical studies of the melting of the Earth's deep matter. Nauka, Moscow. 1991. 312 p
Misra K.C., Anand M., Taylor L.A., Sobolev N.V. Contrib.Mineral.Petrol. 2004. V. 146. P. 696-714.
O'Reilly S.Y., Griffin W.L. Metasomatism and the chemical transformation of rock. 2013. Berlin Heidelberg: Springer. P. 471-533.
Safonov O.G., Butvina V.G. Geochem. Intern. 2016. V. 54. P. 858–872.
Sokol A.G., Kruk A.N., Palyanov Yu.N, Sobolev N.V. Contrib. Mineral. Petrol. 2017. DOI:10.1007/s00410-017-1341-5

Gorbachev N.S., Kostyuk A.V., Gorbachev P.N., Sultanov D.M. Distribution of elements between phlogopite and carbonate at P = 2.8 GPa, T = 1250°C. UDC 550.4.02.

D.S. Korzhinskii Institute of Experimental Mineralogy RAS
142432 Akademica Osip'yana str., 4, Chernogolovka, Moscow dist

Abstract. The distribution of elements between phlogopite Phl and silicate-carbonate melt L_{Cb} was studied at P = 2.8 GPa, T = 1250°C in the presence of H_2O+CO_2 fluid. Concentrations of trace elements in Phl and L_{Cb} were determined by ICP MS. The distribution coefficients of trace elements between Phl and L_{Cb} ($D_{Phl/L_{Cb}}$) vary from 0.001 to 100 or more. High affinity to Phl, $D_{Phl/L_{Cb}}$ of order 100, characterized by highly charged elements, such as Nb, Hf; less affinity to Phl, $D_{Phl/L_{Cb}} \sim 5–8$ have Ta, Zr. Some of elements, P, Na, Ca and REE with $D_{Phl/L_{Cb}} \leq 0.01$, are among the most incompatible with Phl elements. $D_{Phl/L_{Cb}}$ vary from 0.01–0.04 LREE up to 0.2–0.4 HREE. Significant variations in the $D_{Phl/L_{Cb}}$ of elements between Phl and L_{Cb} indicate that in the metasomatized upper mantle, the formation of Phl and L_{Cb} can occur fractionation of trace elements. Ratios of elements with contrast values such as Li/Rb, Rb/Sr, LREE/HREE, Zr/Hf Can serve as indicators of Phl fractionation in carbonate melts.

Keywords: phlogopite, carbonate, distribution of elements, experiment

Introduction. Phlogopite (Phl) is found in magmatic rocks of different genesis, being a source of potassium, as well as chlorine, fluorine, and water. It is also an important indicator of mantle metasomatism, as evidenced by its wide development in xenoliths of metasomatized peridotites and eclogites (O'Reilly, Griffin, 2013). Phlogopite in such xenoliths is formed as a result of interaction with potassium aqueous fluids (Misra et al., 2004). An overview of the reactions occurring during this interaction was made in the work of Safonov, Butvina, 2016. The results of experimental modeling of phlogopite formation in the interaction of peridotite with potassium fluids at high pressures are presented in a number of works (Brey et al., 2011; Sokol et. al., 2017). At 3 GPa, the main phase, the decomposition of which leads to the formation of phlogopite, is found to be garnet: forsterite + pyrope + K-C-O-H (carbonate melt) = phlogopite + enstatite + magnesite. There are also experimental data on the distribution of rare elements between the carbonate melt and the rock-forming minerals of peridotites (Hammouda et al., 2009; Girnis et al., 2006). The purpose of this work was to experimentally study the interphase distribution of the main and secondary elements in the system of phlogopite – carbonate – $H_2O + CO_2$ fluid.

Experimental and analytical methods. The experiments were carried out in Pt ampoules on anvil-with-hole apparatus (NL – 40) in IEM RAS using the quenching technique. Powders of specially prepared mixtures of phlogopite + carbonate ± oxalic acid dihydrate $H_2C_2O_4 \cdot 2H_2O$ as a source of H_2O + CO_2 fluid were placed in an ampoule, which was hermetically sealed. The carbonate fraction consisted of 50 wt.% of Kovdor calcite carbonatite, 30 wt.% of Na_2CO_3, 20 wt.% of K_2CO_3, and 10 wt.% of $H_2C_2O_4 \cdot 2H_2O$ (in relation to the carbonate fraction). The ratio of Na_2O/K_2O = 1.15. The weight ratio of Phl – Cb is 1:1. The temperature was measured by $Pt_{70}Rh_{30}/Pt_{94}Rh_6$ thermocouple. The pressure at high temperatures was calibrated using quartz – coesite equilibrium. The accuracy of determining the temperature and pressure in experiments is estimated at ± 5 °C and ± 1 kbar (Litvin, 1991). The duration of the experiments was 8 hours. Polished preparations of experimental samples were studied on a CamScan MV2300 electron scanning microscope. The concentrations of trace elements in the phlogopite and carbonate fraction in experiments with H_2O+CO_2 fluid were determined by ICP MS. Phl and Cb fractions of quenching samples were separated by chemical methods. The correlation coefficients between measured concentrations in the standard and reference concentrations of elements in it, as well as between concentrations measured in 2 parallel samples > 0,9.

Results. In the system phlogopite–carbonate–H_2O+CO_2, during eutectic melting, phlogopite coexisted with an alkaline silicate-carbonate melt. Quenching samples with a massive texture consisted of elongated corroded phlogopite crystals composing the basic weight of the sample. The intergranular space is filled with a carbonate material of composition 42–45 wt.% CaO, up to 9 wt.% Na_2O, up to 6 wt.% K_2O and SiO_2, the ratio $Na_2O/K_2O \sim$ 1.6 (Fig. 1, Table 1). Phlogopite and carbonate are homogeneous; no inclusions of phlogopite in carbonate and carbonate in phlogopite were found. Table 1 shows the concentrations of rock-forming oxides in coexisting phlogopite and carbonate

(microprobe data), in fig. 1 separation factors for rock-forming oxides between them.

MgO, Al_2O_3 have the maximum affinity for phlogopite. The $D^{Phl/LCb}$ oxides of these metals are greater than 100. SiO_2, FeO, TiO_2, K_2O, $D^{Phl/LCb}$, greater than 1, less than 10, have a moderate affinity for phlogopite. Moderately incompatible with phlogopite Na_2O, $D^{Phl/LCb}$, ~ 0,12, strongly incompatible P_2O_5, CaO – $D^{Phl/LCb}$, less than 0,1. In fig.2 shows the partition coefficients of microelements $D^{Phl/LCb}$ between phlogopite and carbonate melt, in two samples of the same experimental sample, expressed as the ratio of weight concentrations of each element of phlogopite to its concentration in the carbonate melt. Since in the course of the experiment phlogopite could be contaminated with carbonate and carbonate with phlogopite, the ICP MS analysis of Phl and Cb fractions could not exclude distortion of analyzes due to contamination. However, on the microprobe Phl inclusion in Cb and Cb in Phl were not observed. In addition, the concentration of Ca, the main component of Cb, in Phl did not exceed the concentration in the original Phl. There was also no increase in Ti, the typomorphic component Phl, in Cb. Therefore, phlogopite and carbonate do not contain significant amounts of mineral impurities. In this case, the ICP MS analysis data can be considered quite correct.

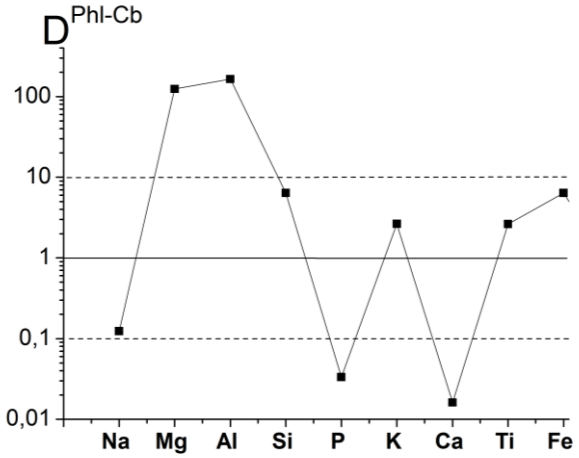

Fig.1. The distribution coefficients of oxides between phlogopite and carbonate.

Table 1. Chemical compositions of phlogopite and carbonate**.**

Phase	SiO_2	TiO_2	Al_2O_3	FeO	MgO	CaO	Na_2O	K_2O	P_2O_5	Total
Phl	39.11	0.68	16.13	0.17	25.73	0.55	1.63	11.13	0.19	94.94
L_{Cb}	6.85	0.26	0.10	0.05	0.23	44.69	7.82	4.17	5.08	69.50
$D^{Phl/Lcb}$	5.71	2.16	161	3.4	112	0.01	0.18	2.67	0.04	69.68
The composition of the original phlogopite										
$Phl_{исх}$	38.66	0.96	13.75	6.01	23.22	0.13	0.42	10.44	-	93.77

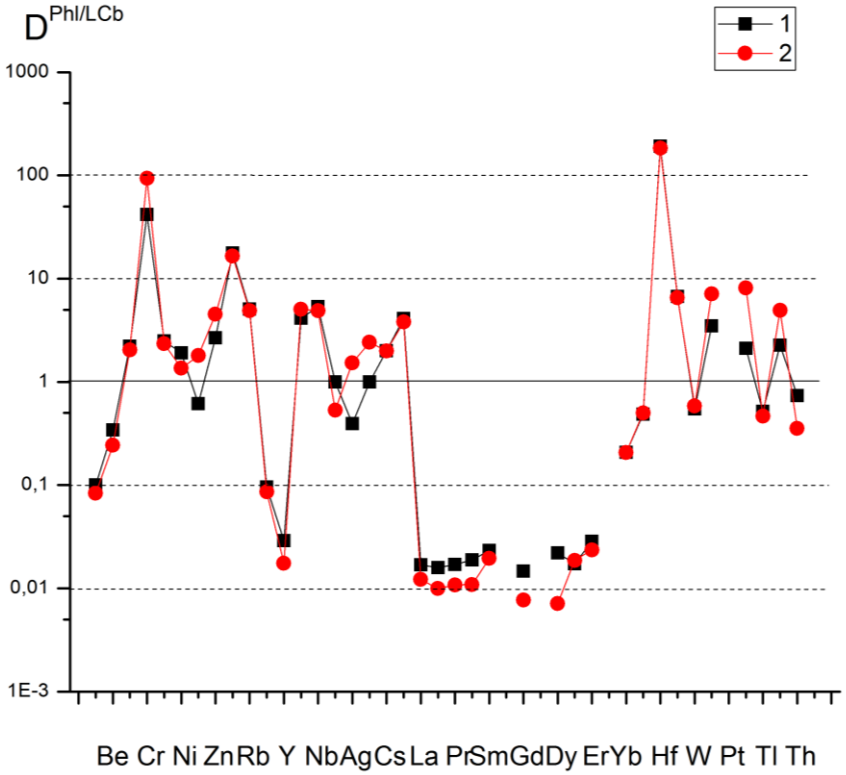

Fig. 2. The distribution coefficients of elements between phlogopite and silicate-carbonate melt in parallel samples of the same sample (1 and 2)

As it can be seen from Fig. 2 for most microelements the separation factors $D^{Phl/LCb}$ vary from 0,01 to 10. High affinity to Phl, $D^{Phl/LCb} > 1$ is characterized by alkaline, alkaline earth, high-charge (Hf, Ta, U) and siderophilic elements (Ni, V), as well as transition metals (Sc, V, Mn). Litophilic elements (Li, Na, Mg, K, Sr, Ba, Pb) have a high affinity to carbonate ($D^{Phl/LCb} < 1$). Sharply stands out high values of hafnium (198 ± 4) $D^{Phl/LCb}$. The distribution of rare earth elements (REE) is characterized by a number of features. In general, REE are among the most incompatible with phlogopite elements, $D^{Phl/LCb}$ are in the range of 0,01 ± 0,03. The exceptions are heavy REE, Yb, Lu, $D^{Phl/LCb}$ of which is an order of magnitude higher than 0,2–0,4. If the ratio of light to medium REE La/Sm is close to 1, then the ratio of light to heavy REE, for example, La/Yb increases to 10.

Discussion and conclusions. Thus, in the system phlogopite – carbonate– ($H_2O + CO_2$), in the process of eutectic melting, phlogopite coexists with an alkaline silicate – carbonate melt. Phlogopite is enriched with alkaline and alkaline-earth, high-charge and siderophilic elements, depleted in rare-earth elements and Y. As indicators of fractionation processes in the phlogopite – carbonate melt – fluid system, pairs of elements with a contrast distribution are of interest, for example, Li/Rb, Rb/Sr, light/heavy REE. High separation factors Hf compared to Zr and other high-charge elements Ta, W, Re should lead to the depletion of carbonate melt with hafnium, an increase in the Zr/Hf ratio in it, which is used as a test for carbonate metasomatism of the upper mantle (Dupuy et al., 1992). In our experiments, the Zr/Hf ratio in the melt is 77 ± 2, in the Kovdor carbonate – 20, Tikshe-Ozero – 102, in the high-bar carbonatites of the Tromso region – 16.4 (Shapovalov et al., 2015). Since the distribution coefficients of light and medium REE between phlogopite and carbonate melt vary within relatively narrow limits, taking into account the significant differences $D^{Phl/LCb}$ of light and heavy REE, it can be expected that a gentle trend of light and medium REE concentrations should be observed in the carbonate melt towards lower values in heavy REE. In general, at pressures up to 4 GPa, temperatures up to 1300 °C, under conditions close to the mantle adiabat, phlogopite remains stable in the presence of alkaline-carbonate fluids and silicate-carbonate melts.

The reported study was funded by RFBR, project number 17-05-00930a

References

Brey G.P., Bulatov V.K., Girnis A.V. Chem. Geol. 2011. V. 281. P. 333–342.

Dupuy C., Liotard J.M., Dostal J. Geochimica et Cosmochimica Acta. 1992. V. 56. P. 2417–2223.

Girnis A., Bulatov V., Lahaye Y., Brey G. Petrology. 2006. V. 14. P. 492–514.

Hammouda T., Moine B., Devidal J., Vincent C. Physics of the Earth and Planetary Interiors. 2009. V. 174. P. 60–69.

Misra K.C., Anand M., Taylor L.A., Sobolev N.V. Contrib.Mineral.Petrol. 2004. V. 146. P. 696-714.

O'Reilly S.Y., Griffin W.L. Metasomatism and the chemical transformation of rock. 2013. Berlin Heidelberg: Springer. P. 471-533.

Safonov O.G., Butvina V.G. Geochem. Intern. 2016. V. 54. P. 858–872.

Sokol A.G., Kruk A.N., Palyanov Yu.N, Sobolev N.V. Contrib. Mineral. Petrol. 2017. DOI:10.1007/s00410-017-1341-5

Litvin Yu.A. Physical and chemical studies of the melting of the Earth's deep matter. Nauka, Moscow. 1991. 312 p

Yu.B. Shapovalov, N.S. Gorbachev, A.V. Kostyuk, and D.M. Sultanov. Doklady Earth Sciences, 2015, Vol. 463, Part 2, pp. 833–838. DOI 10.1134/S1028334X15080139

Iskrina A.V.[1,2], Spivak A.V.[2], Bobrov A.V.[1,2,3], Dubrovinsky L.S.[4], Eremin N.N.[1], Marchenko E.I.[1]. Experimental study of calcium-ferrite structure type phases in the mg-al-cr-o system at conditions of the earth's transition zone and lower mantle UDC 549.02

[1]Lomonosov Moscow State University, Moscow, [2]D.S. Korzhinskii Institute of Experimental Mineralogy RAS, Chernogolovka, [3]Vernadsky Institute of Geochemistry and Analytical Chemistry RAS, Moscow, [4]Bavarian Research Institute of Experimental Geochemistry and Geophysics (BGI) Bayreuth, Germany (grigoryeva_av888@mail.ru)

Abstract: The phases $Mg(Al,Cr)_2O_4$ and $Mg(Cr,Al)_2O_4$ were synthesized in the Mg-Al-Cr-O system. These compounds were studied by optical microscopy, SEM and microprobe analysis. The structures were refined by the method of single-crystal X-ray diffraction. For the first time the Raman spectra for $Mg(Cr,Al)_2O_4$ was obtained. Both studied phases are stable in the transition zone and lower mantle and can be considered as potential aluminum concentrators in the Earth's deep geospheres.

Keywords: phase relations, postspinel phases, transition zone, lower mantle, HP-HT experiment, aluminum

The structure and composition of the Earth's deep geospheres are still debatable and actual problems in geology (Oganov et al., 2005). At the present time , the structure and composition models of the Earth's deep layers have been justified based on geophysical data and analytical data of the mineral composition of deep xenoliths and inclusions in diamonds, theoretical calculations and experimental studies of phase transformations of minerals as well (Irifune and Ringwood, 1993; Walter et al., 2008; Harte, Richardson, 2012). In these models, phases with AB_2O_4 stoichiometry and calcium-ferrite type (CF)

structure are considered as post-spinel phases in the transition zone and lower mantle of the Earth.

The various cations, such as Cr, Al, Mg, Fe, Ca, Ti, Fe and Na, could include in phases with CF-structure and form the solid solutions systems. Therefore composition of natural post-spinel phases is not homogeneous (Kaminsky, 2017). Today several end members of solid solutions (e.g. $NaAlSiO_4$, $MgAl_2O_4$, $CaCr_2O_4$, and $FeCr_2O_4$) are known (Liu, 1977; Irifune et al., 1991; Chen et al. 2003). It is assumed that aluminates with a CF-structure could be host-aluminum phases at the conditions of the Earth's transition zone and lower mantle (Eremin et al., 2016).

The main goal of this work is experimental study of HP-phases of the Mg-Al-Cr-O system at the conditions of the transition zone and the lower mantle.

The experiments were carried out using a 1000-t multi-anvil Sumitomo press at the Bayerisches Geoinstitut (Bayreuth, Germany). Starting materials were powder mixtures of chemically pure oxides MgO, Al_2O_3 and Cr_2O_3 at stoichiometric proportions (1:0.3:0.7 and 1:0.7:0.3). The powders were homogenized in the agate mortar and then annealed in platinum crucibles for 24 hours at 1000°C. The ready starting mixture was placed into a capsule made of a 0.25 mm platinum foil. Experiments on multi-anvil press were carried out using standard 10/5 and 7/3 assemblages. The $Mg(Al,Cr)_2O_4$ and $Mg(Cr,Al)_2O_4$ phases were synthesized at pressures of 12, 14, 18 and 22 GPa and a temperature of 1600˚C with an exposure time from 1 to 5 hours. The phase composition was determined using a scanning electron microscope CamScanM2300 (VEGA TS 5130MM) with the Link INCA spectral analyzer in the IEM RAS. The accelerating voltage was 20 kV. The beam current was ~10nA. The average of compositions of the studied phases was determined by 8 analyses.

The structure of newly formed phases was determined by single-crystal X-ray diffraction using a Bruker SMART APEX CCD diffractometer with Rigaku rotating anode (Rotor Flex FR-D, Mo-Kα radiation) and Osmic focusing X-ray optics at the Bayerisches Geoinstitut, Germany.

Raman spectra of experimental samples were obtained using an Acton SpectraPro-2500i spectrograph with a CCD Pixis2K cooling detector up to -70°C and an Olympus microscope with a 532 nm monomeric laser at IEM RAS.

The samples of phase $Mg(Al,Cr)_2O_4$ with a prevailing aluminum content (> 41 wt.%) were obtained at 12 and 14 GPa. The size of the obtained phase did not exceed 30 μm, thus further work with these samples was difficult.

The $Mg(Al,Cr)_2O_4$ and $Mg(Cr,Al)_2O_4$ phases were synthesized in experiments at pressures of 18 and 22 GPa. The $Mg(Al,Cr)_2O_4$ phase is a green homogeneous crystals 30-100 μm. Composition of the newly formed phase is MgO-38.28; Al_2O_3-30.67; Cr_2O_3-31.05 wt.% ($Mg_{1.541}Al_{0.976}Cr_{0.663}O_4$). This phase has a CF-type structure, orthorhombic syngony, and *Pnma* space group.

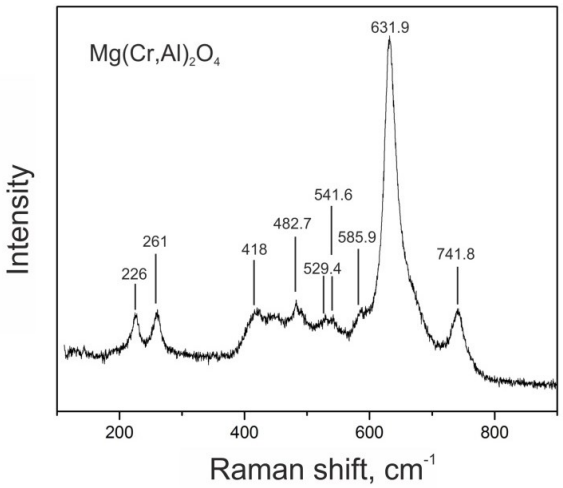

Fig. 1. Raman spectrum for $Mg(Cr, Al)_2O_4$ phase.

The $Mg(Cr,Al)_2O_4$ phase has a rich green color due to the higher chromium content than in the previous phase. The obtained sample is homogeneous, there are crystals ranging in size from 20 to 100 μm with the composition MgO - 22.56; Al_2O_3 - 16.27; Cr_2O_3 - 61.17 wt% ($Mg_{0.997}Cr_{1.434}Al_{0.569}O_4$). The studied phase has the calcium-titanate type (CT) structure, orthorhombic syngony and *Cmcm* space group. Additional information about the structure is listed in Table 1. The Raman spectrum was obtained for the $Mg(Cr, Al)_2O_4$ phase and the positions of the main peaks were determined (Fig. 1).

Table 1. Crystal data for $Mg(Cr,Al)_2O_4$ phase.

	$Mg(Cr,Al)_2O_4$ (rhomb.)
Formula	$Mg_{0.997}Cr_{1.434}Al_{0.569}O_4$
Space group	*Cmcm* (63)
Cell parameters	
a	2.8328
b	9.3956
c	9.5898
α	90°
β	90°
γ	90°
V	255.2407
Z	4
ρ (g/cm^3)	4.5035

In a series of experiments with a sequential change of contains of $MgAl_2O_4$ and $MgCr_2O_4$ end members, there is a structural transition from the CF-structure phase to the CT phase at the increase of chromium component content in $Mg(Al,Cr)_2O_4$ solid solution (Funamori et al., 1998)..

$CaFe_2O_4$ (CF) has a *Pnma* space group, while $CaTi_2O_4$ (CT) has a centered cell and a *Bbmm* (or *Cmcm*) space group. In the first structure, the positions of Mg atom in the tunnel centers are slightly "crimped" (towards the nearest tunnels), while in the second structure with a centered cell, the Mg-positions are strictly aligned (Eremin et al., 2016).

In the newly formed $Mg(Al,Cr)_2O_4$ phase the content of aluminum is higher than chromium, so the sample has CF-type structure, like the $MgAl_2O_4$ end member (Akaogi et al., 1999). When the chromium content increases, the structure of $Mg(Cr,Al)_2O_4$ changes and transfers to the CT-type structure. Refinement of specific structural transition parameters needs further research.

As a result of experimental studies of phase relations in the Mg-Al-Cr-O system, it was found that new phases ($Mg_{1.541}Al_{0.976}Cr_{0.663}O_4$) and ($Mg_{0.997}Cr_{1.434}Al_{0.569}O_4$) are formed in this system, which crystallized with the CF- and CT-type structure, respectively.

It is shown that the newly formed aluminates are stable at wide pressures range 12-22 GPa and 1600˚C, that is suitable to the *PT*-parameters of the transition zone. The studied phases could be considered as post-spinel phases and as aluminum concentrator phases in the deep layers of the Earth.

This work was carried out within the scientific plan of the Laboratory of deep geospheres of the Lomonosov Moscow state University and within the Research Program of the D.S. Korzhinskii Institute of Experimental Mineralogy Russian Academy of Sciences (AAAA-A18-118020590140-7).

References

Akaogi M., Hamada Y., Suzuki T., Kobayashi M., Okada M. High pressure transitions in the system $MgAl_2O_4$–$CaAl_2O_4$: a new hexagonal aluminous phase with implication for the lower mantle// Phys Earth Planet Int.1999. 115. P. 67–77.

Chen M., Shu J., Mao H.-K., Xie X., Hemley R. J. Natural occurrence and synthesis of two new postspinel polymorphs of chromite //PNAS. 2003. 100(25). P. 14651–14654.

Eremin N. N., Grechanovsky A. E., Marchenko E. I. Atomistic and ab initio modeling of $CaAl_2O_4$ high-pressure polymorphs under Earth's mantle conditions// Crystallography Reports. 2016. 61(3). P. 432–442.

Funamori N., Jeanloz R., Nguyen J. H., Kavner A., Caldwell A.W. High-pressure transformations in $MgAl_2O_4$// J Geophys Res. 1998. 103. P. 20813—20818.

Harte B., Richardson S. Mineral inclusions in diamonds track the evolution of a Mesozoic subducted slab beneath West Gondwanaland// Gondwana Research. 2012. 21. P. 236-245.

Irifune, T., Fujino, K., & Ohtani, E. A new high-pressure form of $MgAl_2O_4$// Nature. 1991. 349 (6308), P. 409–411.

Irifune, T., & Ringwood, A. E. Phase transformations in subducted oceanic crust and buoyancy relationships at depths of 600–800 km in the mantle// Earth and Planetary Science Letters. 1993. 117(1–2), P. 101–110.

Kaminsky F.V. The Earth's Lower Mantle: Composition and Structure// Springer Geology. 2017. P. 340.

Liu L. High pressure $NaAlSiO_4$: The first silicate calcium ferrite isotype// Geophysical Reseach Letters. 1977. 4(5). P. 183–186.

Oganov A.R., Price G.D., Scandolo S. Ab initio theory of planetary materials // Z. Kristallogr. 2005. Bd. 220. S. 531-548.

Walter M.J., Bulanova G.P., Armstrong L.S., Keshav S., Blundy J.D., Gudfinnson G., Lord O.T., Lennie A.R., Clark S.M., Smith C.B., Gobbo L. Primary carbonatite melt from deeply subducted oceanic crust// Nature. 2008. 454. P. 622-626.

Kogarko L.N. Crystallization of alkaline phosphates from magmatic melt. UDC 553.491.8:549.271(571.5)

Vernadsky Institute of Geochemistry and Analytical Chemistry, Russian Academy of Sciences, Moscow, 119991 Russia *e-mail: kogarko@geokhi.ru

Abstract: Apatite is the main, practically phosphate mineral of igneous rocks. At the same time, numerous high-temperature phosphate phases of more complex composition are known: silicophosphates (silikovrnotite $Ca_5P_2SiO_{12}$, nagelschmidtite – $Ca_7P_2Si_2O_{16}$, etc.), observed in the basic fluorine metallurgical slags (Lapin, 1956), as well as double phosphates: renanite ($CaNaPO_4$) – calcium orthophosphate ($Ca_3(PO_4)_2$) occurr in products of high-temperature phase processing of apatite with sodium carbonate (Gunawardane, Glasser, 1979; Niragu et al., 1984).

We experimentally studied the phase diagram $NaAlSiO_4$ (nepheline) – $Ca_5(PO_4)_3$ (apatite) -$CaMg(Si_2O_6)$ (diopside). In the Apatite-nepheline section, we found double phosphate $NaCaPO_4$, which is stable in the high-temperature region. The closest natural analogue of this phase is arctite mineral $Ca_4Na_2(PO_4)_3$.

The main reason for the absence of double phosphate in natural igneous rocks is probably that they are crystallized only at sufficiently high concentrations of phosphorus in the melt (>6 wt. % P_2O_5), which is not possible in magmas in the temperature range of stability of this mineral.

Keywords: *Magmatic phosphates; Phase diagram apatite-nepheline-diopside; Apatite; Arctite.*

Apatite is practically the only phosphate mineral in igneous rocks. At the same time, there are numerous high-temperature phosphate minerals of a more complex composition - silicophosphates (silicocarnotite - $Ca_5P_2SiO_{12}$, nagelschmidtite - $Ca_7P_2Si_2O_{16}$, etc.), observed in the main phosphorous metallurgical slags (Lapin, 1956), as well as binary phosphates (CaPaO) of the system calcium

($Ca_3(PO_4)_2$), which are found in the products of high-temperature solid-phase processing of apatite with sodium carbonate (Gunawardane and Glasser, 1979; Niragu et al., 1984). Similar double phosphates were found in meteorites: buchwaldite ($CaNaPO_4$) (Olsen et al., 1977) and merrillite ($3CaO \cdot Na_2O$ X P_2O_5) (Chervinsky, 1941).

The release of complex phosphates in equilibrium with an aluminosilicate melt was observed by us in the systems nepheline - fluorapatite (Kogarko, 1971) and nepheline - diopside - fluorapatite (Kogarko et al., 1984), as well as from melts of ijolite-urtite composition with apatite, to which a small amount of one of the oxides Na_2O, K_2O or CaO (Kogarko et al., 1987). The phosphate mineral crystallizes as the first liquidus phase. Crystals, as a rule, are round in shape, 1-2 mm in size are grouped in the form of "flowers", bunches, or give dendrite clusters (Fig. 1). Crystals of pale blue color, uniaxial, negative with refractive indices ng = 1.597 and np = 1.592, readily soluble in hydrochloric acid.

The chemical composition of the mineral was determined using the SAMEVAKh microprobe. Since the analysis for fluorine requires a long exposure, the composition was determined in two stages: first, the mineral was analyzed for all elements except fluorine, then fluorine was determined separately. Fluorapatite was used as a standard. The compositions of phosphates and melts in equilibrium with them are given in the table.

As can be seen from Table 1, the obtained artificial mineral is a double phosphate of calcium and sodium. In addition to these elements, silicon, magnesium, iron, fluorine and potassium are present in small amounts, and the content of the latter increases with an increase in its concentration in the melt. The amount of fluorine entering the mineral, on the contrary, does not depend on the concentration of this element in the melt and amounts to ~ 1 wt%.

It follows from the analysis data that the obtained double phosphate is a phase of variable composition, the main minerals of which are $NaCaPO_4$ and $Ca_3(PO_4)_2$. The ratios of these components vary from 2.6 to 5.0. In addition, ~ 2 wt% CaF_2 and Ca_2SiO_4 are constantly present in the crystals, the content of which varies from 2 to 12 wt%, and the highest concentrations of this endpoint are observed in crystals in equilibrium with high-calcium melts. The limited amount of available experimental data does not allow one to reveal the quantitative relationships between the compositions of the melt and crystals.

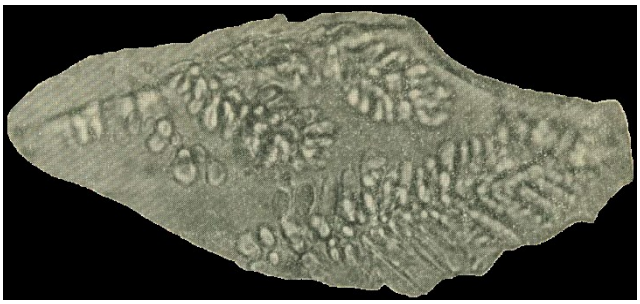

Fig.1. Crystals of double phosphate in glass of ijolite-urtite composition T 1300°C, composition 4 (see table 1).

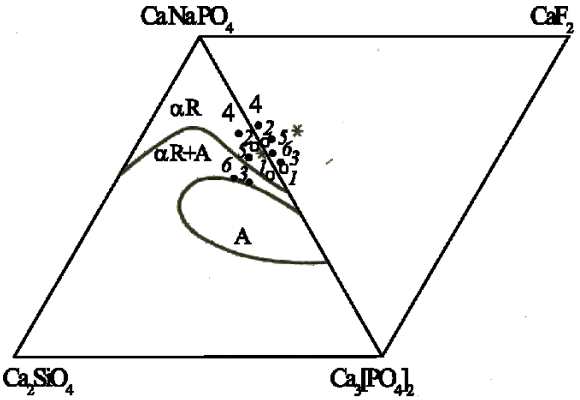

Fig.2. Position of double phosphates on the $CaNaPO_4 - Ca_2SiO_4 - Ca_3(PO_4)_2 - CaF_2$ diagram. The numbers correspond to the sample number in the table. The asterisk indicates arctite. Phase fields on the phosphate triangle after (Berak, Znamierowska, 1973) for 1300°C.

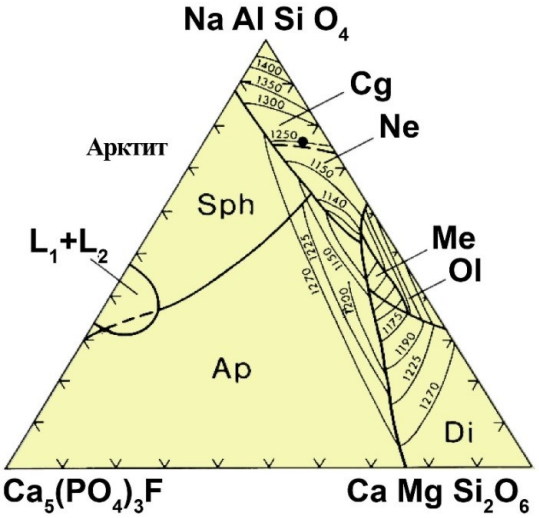

Fig. 3. Phase relationships in the system $NaAlSiO_4$ - $CaMgSi_2O_6$ – $Ca_5(PO_4)_3F$ at 1 atm. pressure (Kogarko, 1977). Cg - carnegite, Ne - nepheline, Ol - olivine, Me - melelite, Di - diopside, Ap - apatite, in Sph - arctite, $L_1 + L_2$ - two immiscible liquids, • - average composition of apatite-nepheline intrusion.

Table 1. Compositions of double phosphates and melts in equilibrium with them, wt%.

Composition	1 (1450°C)		2 (1400°C)		3 (1300°C)		4 (1300°C)		5 (1300°C)		6(1300°C)		
	phosphate	melt	phosphate	melt	phosphate	melt	phosphate	melt	phosphate	melt	phosphate	melt	Apatite
SiO_2	0,83	31,17	0,69	34,32	3,33	33,68	1,41	36,10	1,70	35,29	4,09	32,68	1,20
TiO,	—	—	—	—	0,01	1,67	0,05	2,65	0,03	2,38	0,04	1,71	0,04
Al_2O_3	0,20	25,83	0,12	29,08	0,07	15,85	0,16	18,78	0,15	18,22	0,06	15,40	0,05
FeO	—	—	—	—	0,17	5,10	0,25	5,82	0,27	5,54	0,21	4,98	0,23
MgO	—	—	—	—	0,38	1,91	0,45	1,45	0,36	1,31	0,33	1,87	0,02
CaO	43,46	18,07	42,31	12,79	43,92	23,40	40,40	13,79	41,51	13,28	44,21	24,87	55,08
Na_2O	10,82	12,46	12,38	15,07	9,87	8,27	12,73	10,78	11,07	8,35	10,13	8,12	0,28
K_2O	—	—	—	—	1,08	3,26	0,91	4,08	2,03	8,81	1,08	3,06	0,10
P_2O_5	43,63	11,21	43,47	7,83	40,22	6,20	42,68	5,94	41,90	6,17	38,97	6,56	39,71
F	1,03	1,11	0,96	0,70	0,89	0,55	0,91	0,58	0,94	0,57	0,84	0,63	3,24
Phosphate formulations for minals													
$NaCaPO_4$	349	—	399	—	341	—	429	—	400	—	350	—	—
$Ca_3(PO_4)_3$	133	—	107	—	113	—	86	—	95	—	100	—	—
Ca_2SiO_4	14	—	11	—	55	—	23	—	28	—	68	—	—
CaF_2	27	—	25	—	23	—	24	—	25	—	22	—	—

Comparison of the compositions of the obtained crystals and mineral phases of the $NaCaPO_4$ – $Ca_3(PO_4)_2$ – Ca_2SiO_4 system (Fig. 2) shows that the projections of the compositions of the discussed phosphates lie partially in the field of α-renanite solid solutions or in the two-phase region of α-renanite solid solutions + phase A. The resulting mineral cannot be identified either with a solid solution based on renanite, or with phase A, since it differs significantly from the first in optical properties (renanite (buchwaldite) is biaxial, negative with refractive indices ng = 1.616, nm - 1.610 , np = 1.607 (Olsen et al., 1977)), and from phase A - by a higher ratio of the main minerals (for phase A $NaCaPO_4$ / $Ca_3(PO_4)_2$ = 0.5-2.0 (Berak, Znamierowska, 1973; Ando, Matsuno, 1968)), in addition, the mineral always contains, as already mentioned, fluorine, the amount of which is constant and does not depend on the concentration of this element in the melt. The latter, apparently, indicates that fluorine is an essential component of the considered mineral. In this regard, the closest natural analogue of the mineral is arctite, discovered and studied by A.P. Khomyakov et al. (Khomyakov et al., 1981) in an ultra-alkaline pegmatite vein intersecting the ijolite-urtites of the Khibiny massif. Idealized arctite stoichiometry: $Ca_4Na_2(PO_4)_3$. The chemical composition of natural arctite is much more complex (in addition to calcium, sodium and phosphorus, it contains 12% BaO, 3% ZrO_2, 3.6% SiO_2 and 5% F). This mineral is uniaxial, negative with ng = 1.578 and np = 1.577.

The crystallochemical formulas of the minerals studied by us can be expressed as (ordinal numbers in accordance with the table)

1. $Ca_{3.72}Na_{1.66}(PO_4)_3(F_{0.26}O_x)$
2. $Ca_{3.68}Na_{1.95}(PO_4)_3(F_{0.25}O_x)$
3. $(Ca, Mg, Fe)_{3,73}(Na, K)_{1,59}[(P, Si)O_4]_3(F, O)$
4. $(Ca, Mg, Fe)_{3,57}(Na, K)_{1,99}[(P, Si)O_4]_3(F, O)$
5. $(Ca, Mg, Fe)_{3.66}(Na, K)_{1.94}[(P, Si)O_4]_3(F, O)$
6. $(Ca, Mg, Fe)_{3,90}(Na, K)_{1,69}[(P, Si)O_4]_3(F, O)$

or in an idealized form: $Ca_4Na_2(PO_4)_3(O, F)$, i.e., the stoichiometric composition corresponds to arctite, if we neglect some deficiency in the cationic part, which is systematic and goes beyond the analytical error. In addition, the fluorine content of the mineral is significantly lower than in the idealized formula.

Studies of the solubility of apatite in aluminosilicate melts of various compositions (Kogarko et al., 1987) showed that crystallization of

binary phosphates is observed only from melts, the total alkali content of which exceeds 11% at a P_2O_5 concentration> 6%. The temperature range of stability of double phosphates is determined by the composition of the melt. In the apatite - nepheline system (Kogarko, 1971), crystallization begins at a temperature of 1500°C and continues (with or without apatite) up to T solidus (1270°C). In the triple system apatite - nepheline - diopside, the stability field of double phosphate also covers the high-temperature region of the system, and it is the first liquidus phase. With a decrease in T, apatite is added to it, and in the low-temperature region (below 1125°C), double phosphate was not found in the quenching products. Apparently, as T decreases, the double phosphate reacts with the melt to give apatite. A similar picture is observed for ijolite-urtite melts. For composition 4 (Table 1), the first crystals of double phosphate appear at a temperature of - 1375°C, then at 1200 ° C the first crystals of apatite appear and the joint crystallization of two mineral phases is observed at least up to 1078°C, and as T decreases, the ratio between the amount of double phosphate and apatite so that at 1078°C only single precipitates of double phosphate occur against the background of well-faceted numerous crystals of apatite.

The main reason for the absence of double phosphate in natural igneous rocks is probably that it crystallizes only at sufficiently high phosphorus contents in the melt (> 6 wt% P_2O_5), which are not reached in magmas in the region of stability temperatures of this mineral.

SOURCE OF FINANCING The work was carried out within the framework of the topic under state assignment No. 0137-2019-0014

References

Ando J., Matsuno S. (1968). $Ca_3(PO_4)_2$–$CaNaPO_4$ system // Bull. Chem. Soc. Jap. Vol. 41. P. 342-347.

Berak J., Znamierowska T. (1973) Phase equilibria in system CaO– Na_2O–P_2O_5. 4. Partial system CaO–$Ca_2P_2O_7$–Na_2O // Roczniki Chemii Ann. Soc. Chim. Polonorum. Vol. 47. P. 1137-1148.

Chervinskiy P.N. (1941) // Meteoritika. T. 2. P. 83-88. [in Russian].

Gunawardane R. P., Glasser F.P. (1979). Reaction of chlorapatite, $Ca_5(PO_4)_3(Cl, F)$ with sodium carbonate and silica // J. Materials Sci. Vol. 14. P. 2797 - 2810.

Khomyakov A.P., Bykova A.V., Kurova T.A. (1981) // Zap. Vsesoyuz. mineral, o-va. № 4. P. 506-511. [in Russian].

Kogarko L.N. (1971). Fazovyye ravnovesiya v sisteme nefelin - F-apatit // Geokhimiya. № 2. P. 160-168. [in Russian].

Kogarko L.N., Krigman L.D., Belyakova Ye.N. (1984). Sistema nefelin-diopsid-apatit i evolyutsiya rasplavov pri kristallizatsii apatitonosnoy iyolit-urtitovoy magmy // Geokhimiya. № 4. P. 472-477. [in Russian].

Kogarko L.N., Krigman L.D., Krot T.V. (1987). Rastvorimost' i geokhimiya fosfora v magmakh // Geokhimiya. № 7. P. 915-921. [in Russian].

Lapin V.V. (1956) // Tr. In-ta geologii rudnykh mestorozhdeniy, petrografii, mineralogii i geokhimii. Vyp. 2. P. 76-81. [in Russian].

Olsen E., Erlichman J., Bunch T.E. (1977). Buchwaldite, a new meteoritic phosphate mineral // Amer. Miner. V. 62. P. 362-364.

Phosphate Minerals edited by J. O. Nriagu and P. B. Moore. Springer-Verlag, Berlin, (1984). 442 p. DOI: 10.1002/gj.3350200213.

Kostyuk A.V., Gorbachev N.S., Sultanov D.M., Nekrasov A.N. Experimental investigation of peridotite-basalt-$(K, NA)_2CO_3$-H_2O system at $P = 4$ GPa, $T = 1400$ °C: phase composition and critical relationship between melt and fluid. UDC 550.4.02

D.S. Korzhinskii Institute of Experimental Mineralogy RAS 142432 Akademica Osip'yana str., 4, Chernogolovka, Moscow district. nastya@iem.ac.ru, gor@iem.ac.ru, dill@iem.ac.ru, alex@iem.ac.ru

Abstract. New data on the phase relationships in the fluid-containing upper mantle at $P = 4$ GPa, $T = 1400$°C were obtained at partial melting of peridotite-basalt association with an alkaline-carbonate fluid. This system was experimentally studied as a model of the mantle reservoir with protoliths of the subdued oceanic crust. Signs of critical relationships between the carbonated silicate melt and the fluid were observed. The reaction ratios among the minerals of peridotite restite with the substitutions of *Ol* ← *Opx* ← *Ca-Cpx* ← *K-Amf* indicated a high chemical activity of the supercritical liquid. The results of the experiments suggest that in the fluid-containing upper mantle with supercritical *P-T* there are areas of partial melting (asthenosphere lenses), containing near-solidus supercritical liquids enriched with incompatible elements, with high reactivity. Mantle reservoirs with supercritical liquids, similar in geochemical terms to the "enriched" mantle, can serve as a source of magma enriched with incompatible elements. The modal and latent metasomatism of the upper mantle under the influence of supercritical liquids leads to the peridotite refertilization due to the enrichment of restite minerals with incompatible elements.

Keywords: peridotite; basalt; fluid; critical relations; experiment

Introduction. Subduction of oceanic crust is the main mechanism for the exchange of matter between the crust and mantle. It leads to eclogitization of basalts and the formation of reservoirs with protoliths of subducted crust enriched in volatile and incoherent elements in peridotite mantle. The interest in the study of fluid-containing silicate systems at high pressures is determined by the influence of fluids on the phase composition, melting point of the mantle rocks, the composition of the resulting silicate and salt (carbonate, chloride, sulfide) melts. An important feature of fluid-containing silicate systems is the existence at high pressures and temperatures of the critical relationship between silicate melt and fluid,

due to their high mutual solubility. At critical parameters (P_kT_k), complete miscibility is observed between them with the formation of a supercritical fluid, and above the second critical point ($2P_kT_k$) *P–T* – between the crystalline phases, the fluid and the melt, therefore, the solidus in the silicate-fluid system as such is absent (Wyllie, Ryabchikov, 2000; Keppler, Audetat, 2005; Litasov, Ohtani, 2007). To obtain new data on the phase relationships in the upper mantle under supercritical conditions, the peridotite – basalt–(Na, K)$_2CO_3$–H_2O system was experimentally studied at 4 GPa and 1400 °C. Studies of the fluid-containing peridotite-eclogitic system as an experimental model of the mantle reservoir with protoliths of the subducted oceanic crust are of interest for constructing petrogenetic models of magmatism of subduction zones.

Experimental and analytical methods. The experiments were carried out in IEM RAS on the anvil-with-hole apparatus (NL-40) using a quenching technique. A multi-ampoule technique with a combined Pt-peridotite ampoule was used (Gorbachev, 1990). The peridotite ampoule was filled with the initial mixture: tholeitic basalt (~ 80 wt.%), Na_2CO_3 and K_2CO_3 (~ 10 wt.%), pyrrhotine (~ 10 wt.%) and distilled H_2O (~ 20 wt.% relative to silicate). The equipped peridotite ampoule was placed in a platinum ampoule, which was hermetically sealed. The temperature was measured by $Pt_{70}Rh_{30}/Pt_{94}Rh_6$ thermocouple. The pressure at high temperatures was calibrated using quartz – coesite equilibrium. The accuracy of determining the temperature and pressure in experiments is estimated at ±5 °C and ±1 kbar (Litvin, 1991). The duration of the experiments was from 8 to 24 hours. Polished preparations of experimental samples were studied on a CamScan MV2300 electron scanning microscope.

Results of the experiments. Micrographs of the experimental samples are shown in Fig. 1, and the chemical compositions of the coexisting phases are shown in Table 1.

The cross section of the experimental sample (Fig. 1a) shows three zones: 1) the zone of the disintegrated peridotite ampoule (Fig. 1c); 2) the reaction zone at the peridotite – basalt boundary; 3) the basalt zone (Fig. 1b) formed during the quenching of the supercritical fluid. The peridotite zone of the sample consists of isolated relics or intergrowths of olivine, orthopyroxene and clinopyroxene. There are reactionary relationships between them and the newly formed minerals in the sequence: orthopyroxene ← clinopyroxene ← potassium-containing amphibole (Fig. 1 d, e), the formation of quenching phlogopite (Phl) and carbonate (Cb), and aluminosilicate glass (Gl) globule (Fig. 1 f). Fig. 1 (d-f) shows the types of reaction ratios in restite peridotite, and table 1 shows their chemical composition. The reaction zone is represented by the association of difficult-to-diagnose micron-sized phases. The basalt zone consists of a mixture of fine-grained (up to 5 μm) aggregates of silicates and carbonates, sulfide and aluminosilicate microglobules. In contrast to subcritical conditions, silicate glass in the peridotite ampoule does not form.

Table 1. The compositions of coexisting phases in the peridotite-basalt-(Na, K)$_2CO_3$-H_2O system at *T* = 1400 °C, *P* = 4GPa.

Phase	SiO_2	TiO_2	Al_2O_3	Cr_2O_3	FeO	MnO	MgO	CaO	Na_2O	K_2O	Total
Ol	40.23	0.40	0.78	2.36	6.08	0.12	50.20	0.18	0.38	0.04	100.58
K-*Amp*	41.78	0.85	15.02	0.10	6.56	0.21	14.36	10.87	2.09	1.50	93.37
Cpx	45.82	2.04	11.54	0.18	3.77	0.00	11.97	21.69	0.89	0.10	98.16
Opx	54.29	0.28	4.88	1.03	3.54	0.13	33.33	1.69	0.00	0.00	99.17
Phl	40.67	0.35	14.20	0.37	2.89	0.20	21.92	0.06	1.31	6.65	88.89
L_{Sil}- *Gl*	53.08	0.24	18.60	0.04	0.10	0.12	0.00	0.22	6.81	2.83	82.17
L_{Cb}	2.59	0.17	0.72	0.05	0.88	0.48	3.21	42.89	0.89	0.10	52.07

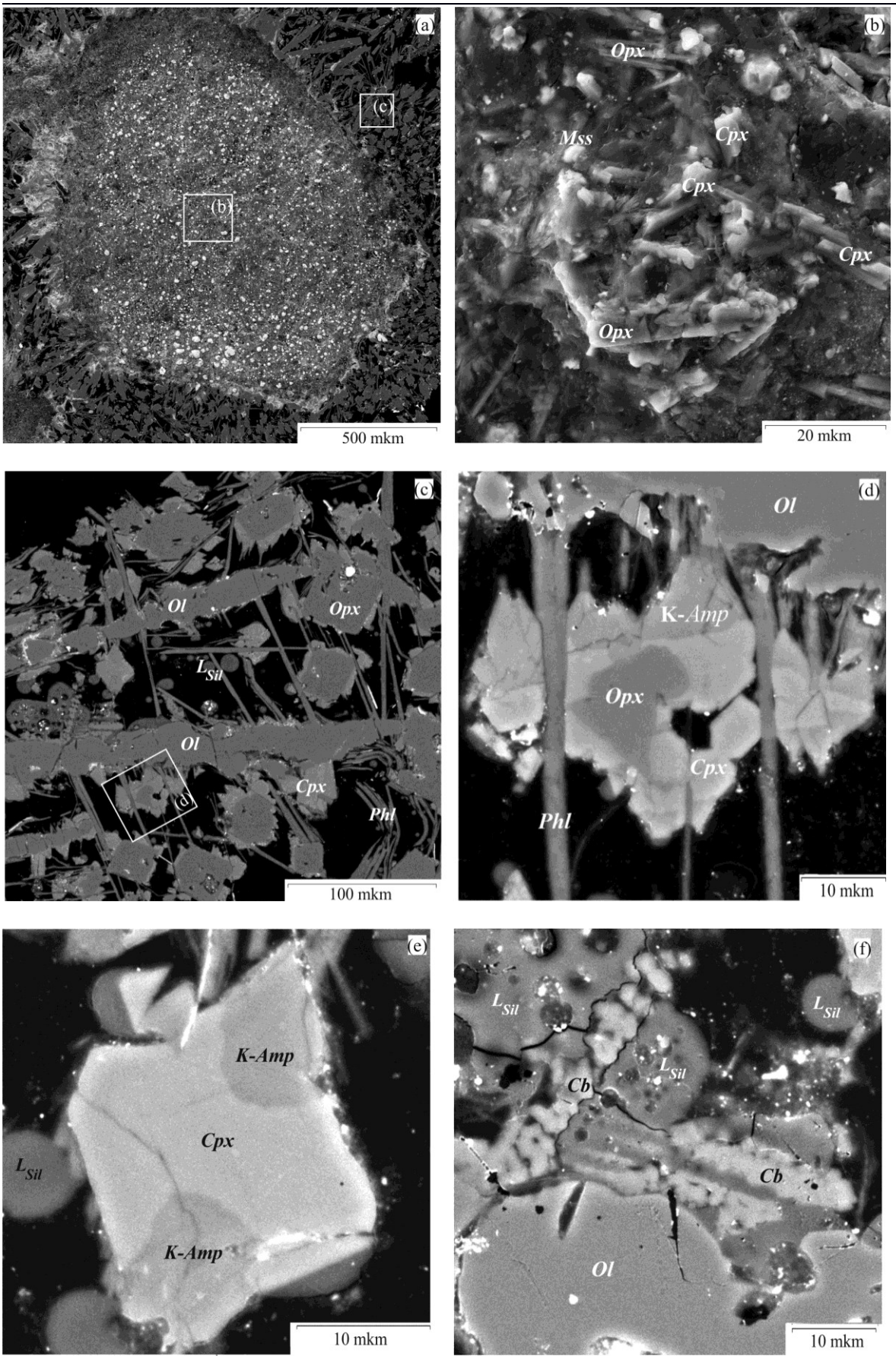

Fig. 1. *Peridotite-basalt-Na_2CO_3-K_2CO_3-H_2O system*. BSE images of experimental run products. (a) peridotite-basalt contact; (b) basalt part, represented by a fine mixture of quenching silicate phases; (c) disintegrated peridotite part; (d-f) different areas of peridotite ampoules, characterizing the features of the phase composition, due to the reaction ratios in the peridotite restead with *Opx* ← *Cpx* ← K-*Amp* substitutions, newly formed *Phl*, *Cb* and quenched glass globules (L_{Sil}).

Discussion and conclusions. Critical ratios between fluid and silicate melt are observed. The interaction of supercritical fluid with restite peridotite minerals leads to the formation of clinopyroxene, K-amphibole, phlogopite, carbonate, quenching silicate globules. The newly formed clinopyroxene and K-amphibole are in reaction ratios with olivine, orthopyroxene and clinopyroxene. As applied to the conditions of the upper mantle, the modal metasomatism under the influence of water-containing supercritical fluids leads to secondary enrichment – the "refertilization" of the depleted rest of the harzburgite composition by replacing the harzburgite olivine-orthopyroxene association with the newly formed phlogopite-clinopyroxene association. The peculiarities of the texture and phase composition of the samples under supercritical conditions allow us to conclude that the reservoirs with protoliths of the subdued oceanic crust are zonal. The outer zone is a disintegrated restite of a harzburgite or dunite composition, which has undergone a "referetilization" as a result of the formation of new minerals in it, metasomatically changed under the influence of supercritical fluid. The inner zone is insulated lenses of supercritical fluid. Disintegration of the fluid-containing mantle peridotite substrate at supercritical pressures can lead to the formation of tectonically weakened zones, fluid paths and upper mantle plumes.

The reported study was funded by RFBR, project number 17-05-00930a

References

Gorbachev N.S. Fluid-magma interaction in sulfide-silicate systems. International Geology Review, 1990, 32(8):749-831

Litvin Yu.A. Physical and chemical studies of the melting of the Earth's deep matter. Nauka, Moscow. 1991. 312 p

Keppler H., Audetat A. Fluid-mineral interaction at high pressure. Mineral behavior at extreme conditions // EMU Notes in Mineralogy. 2005. V. 7. P. 225–251.

Litasov K.D., Ohtani E. Effect of mater on the phase relations in Earth's mantle and deep water cycle // Special Paper Geolog. Soc. Amer. 2007. V. 421. P. 115–156.

Wyllie P.J., Rhyabchikov I.D. Volatile components, magmas, and critical fluids in upwelling mantle // Journal of Petrology. 2000. V. 41. P. 1195–1206.